DISCLAIMER

This report was prepared as an account of work sponsored by an agency of the United States Government. Neither the United States Government nor any agency thereof, nor any of their employees, makes any warranty, express or implied, or assumes any legal liability or responsibility for the accuracy, completeness, or usefulness of any information, apparatus, product, or process disclosed, or represents that its use would not infringe privately owned rights. Reference herein to any specific commercial product, process, or service by trade name, trademark, manufacturer, or otherwise does not necessarily constitute or imply its endorsement, recommendation, or favoring by the United States Government or any agency thereof. The views and opinions of authors expressed herein do not necessarily state or reflect those of the United States Government or any agency thereof. Reference herein to any social initiative (including but not limited to Diversity, Equity, and Inclusion (DEI); Community Benefits Plans (CBP); Justice 40; etc.) is made by the Author independent of any current requirement by the United States Government and does not constitute or imply endorsement, recommendation, or support by the United States Government or any agency thereof.

June 2025 – Version 4.2

Sandia National Laboratories

Final Report: Development of a High-Intensity Heat Flux Gauge and Characterization Facility

Luke McLaughlin, Hendrik Laubscher, Nathan Schroeder, Luis Maldonado, Benjamin Bean, Kathryn Small, Jörgen Konings, Robert Dolce, and Kees Van Den Bos

May 2025

a. Federal Agency	Department of Energy - SETO	
b. Award Number	CPS - 38484	
c. Project Title	Extreme Intensity Concentrating Solar Heat Flux Sensor Development & Calibration	
d. Recipient Organization	Sandia National Laboratories	
e. Project Period[1]	Start: *10/01/2021*	End: *03/31/2025*
f. Principal Investigator (PI)	*Hendrik Frederik Laubscher* *hlaubsc@sandia.gov* *+1 (505) 284 4208*	
g. Certifying Official	*Margaret Gordon* *megord@sandia.gov* *+1 (505) 284-9630*	

U.S. DEPARTMENT OF ENERGY

National Nuclear Security Administration

Sandia National Laboratories is a multimission laboratory managed and operated by National Technology and Engineering Solutions of Sandia, LLC, a wholly owned subsidiary of Honeywell International Inc., for the U.S. Department of Energy's National Nuclear Security Administration under contract DE-NA0003525.

Sandia National Laboratories

EXECUTIVE SUMMARY

Sandia National Laboratories (SNL) and Hukseflux Thermal Sensors (HTS) collaborated to advance the design and calibration of high-intensity heat flux gauges capable of measuring 2500 kW/m². An industry trade study was first conducted and highlighted the need for enhanced gauge designs and calibration methodology & services suited for high-intensities and broadband flux. We then developed, tested, and evaluated three prototype gauge designs along with four distinct coating types, each designed to extend the measurable flux range of existing HTS products to higher intensity levels. Following a down selection process, the project team refined the focus to a final product design, incorporating updated features to enhance its robustness during high flux exposure.

The project concluded with the testing and determination of the final product specifications for the optimized gauge design. This effort was accompanied by significant upgrades to the NSTTF Flux Gauge Characterization Facility (FGCF), which included the implementation of traceable reference sensor measurements and enhancements to instrumentation and data collection capabilities. In addition to the technical advancements, the team successfully updated and submitted a publication outlining a proposed high-intensity heat flux calibration method that leverages concentrated solar light.

Project Achievements:

- Conducted an industry trade study identifying the need for improved high heat flux gauge designs exceeding 1000 kW/m², along with calibration methodology and standardization.
- Developed, tested, and evaluated three prototype heat flux gauge designs.
- Investigated the performance and feasibility of four different coating types.
- Selected a final product design through a down-selection process.
- Enhanced the robustness of the gauge design with updated features.
- Conducted comprehensive testing and characterization of the final product design.
- Upgraded the NSTTF Flux Gauge Characterization Facility (FGCF) reference instrument with traceable voltage, resistance, and aperture area measurements.
- Improved FGCF instrumentation and data collection capabilities.
- Updated and submitted a journal publication regarding a proposed high-intensity heat flux calibration method utilizing concentrated solar light.

U.S. DEPARTMENT OF ENERGY

National Nuclear Security Administration

Sandia National Laboratories is a multimission laboratory managed and operated by National Technology and Engineering Solutions of Sandia, LLC, a wholly owned subsidiary of Honeywell International Inc., for the U.S. Department of Energy's National Nuclear Security Administration under contract DE-NA0003525.

DETAILED ACCOMPLISHMENTS

Trade Study

A trade study was conducted to outline the development needs regarding an enhanced high-intensity broadband flux sensor and calibration facility & methodology for both Concentrated Solar Power (CSP) and non-CSP high-intensity flux applications [1]. To gather insights on design and calibration requirements, stakeholders involved in high-intensity flux measurements were surveyed and interviewed. A summary is presented here and full details can be found in [1].

Key stakeholder requirements for the flux sensor included the capability to measure flux levels exceeding 5,000 kW/m², a lifespan of over 1,000 cycles, a response time of less than 500 ms, sustained exposure at maximum flux for over 60 minutes, and a measurement uncertainty of less than 5%. Additionally, stakeholders emphasized the need for minimal cost, short procurement lead times, and effective high-intensity broadband flux calibration.

Table 1. Summary of CSP stakeholder sensor limitations and design requirements. The metric range for each design specification corresponds to the predominant stakeholder response.

Metric/Topic	Predominant Stakeholder Response
Current Limitations	Cost, procurement lead time, robustness at high flux and temperatures, measurement uncertainty, signal noise
Maximum Rated Flux [kW/m^2]	>5,000
Response Time [ms]	250 – 500
Angular Aperture [deg]	>90
Exposure Time at Max Flux [min]	>60
Sensor Lifetime at Max Flux [# cycles]	>1,000
Sensor Sensitivity After Max Exposure [%]	>97.5
Repeatability at Max Exposure [%]	>97.5
Expanded Measurement Uncertainty [%]	<5
Mounting Requirements	Standard flange mounting
Spectral Requirements	Broadband (solar) spectrum
Cooling Requirements	Water and/or glycol
Sensor Coating Requirements	Robust to radiative and convective heat transfer

Metric/Topic	Predominant Stakeholder Response
Sensor Cooling Line and Signal Cable Requirements	Robust cooling lines and cable sheaths. Minimal signal noise contributions.

Table 2. Summary of non-CSP stakeholder sensor limitations and design requirements. The metric range for each design specification corresponds to the predominant stakeholder response.

Metric/Topic	Summary and Metric Response Range
Current Limitations	Lead time, robustness at high flux and temperatures, measurement uncertainty, signal noise, response time, sensor size
Maximum Rated Flux [kW/m2]	2,500 – 5,000
Response Time [ms]	100 – 250
Angular Aperture [deg]	60 – 90
Exposure Time at Max Flux [min]	1 – 30
Sensor Lifetime at Max Flux [# cycles]	500 – 1,000
Sensor Sensitivity After Max Exposure [%]	>97.5
Repeatability at Max Exposure [%]	>97.5
Expanded Measurement Uncertainty [%]	<5
Mounting Requirements	Smaller geometry
Spectral Requirements	Broadband (full) spectrum
Cooling Requirements	Water and/or glycol
Sensor Coating Requirements	Robust to radiative and convective heat transfer
Sensor Cooling Line and Signal Cable Requirements	Robust cooling lines and cable sheaths. Minimal signal noise contributions.

The flux sensor specific needs of CSP and non-CSP stakeholders are combined and summarized as follows:

1. Increased robustness – includes increased exposure duration at high flux
2. Reduced response time
3. Decreased signal noise and measurement uncertainty
4. Reduced cost
5. Decreased procurement lead time

The requirements for the calibration of high intensity broadband flux sensors to be used in CSP and non-CSP applications were determined through industry and R&D stakeholder interviews and surveys. Tables 3 and 4 show high intensity broadband flux sensor calibration requirements expressed by CSP and non-CSP stakeholders, respectively. It is noted that the metric range presented for each design specification corresponds to the predominant stakeholder response.

Table 3. Summary of CSP stakeholder sensor calibration requirements. The metric range for each specification corresponds to the predominant stakeholder response.

Metric/Topic	Summary and Metric Response Range
Current Limitations	Calibration range and non-solar calibration source
Spectral Calibration Requirements	Broadband (solar) spectrum
Calibration Ranges [kW/m2]	>5,000
Calibration Traceability	Traceable measurement to SI units
Calibration Verification	Validated calibration procedure

Table 4. Summary of non-CSP stakeholder sensor calibration requirements. The metric range for each specification corresponds to the predominant stakeholder response.

Metric/Topic	Summary and Metric Response Range
Current Limitations	Calibration range and partial spectrum
Spectral Calibration Requirements	Broadband (full) spectrum
Calibration Ranges [kW/m^2]	2,500 – 5,000
Calibration Traceability	Traceable measurement to basic SI units
Calibration Verification	Validated calibration procedure

The flux sensor calibration needs of CSP and non-CSP stakeholders are combined and summarized as follows:

1. Increased calibration range matching sensor specifications
2. Ability to calibrate over the full or broadband spectrum of radiation
3. Traceable calibration radiation source
4. Metrological traceability of flux measurement to SI units (accreditation not critical)

Current solid-state sensor technologies and accredited calibration facilities were found to fall short of meeting stakeholder requirements for reliable, high-intensity heat flux measurement and calibration. In response, SNL and HTS initiated this collaborative effort to develop a low-cost, robust, and reliable circular foil gauge designed to operate at higher flux levels and improve measurement accuracy and reliability compared to existing models.

To complement the sensor development and address stakeholder calibration needs, SNL sought to establish a high-intensity broadband flux sensor calibration facility at the NSTTF. This facility

utilizes an existing solar furnace capable of concentrating solar flux up to 6,000 kW/m² within a 5 cm diameter focal plane. Upgrades were planned to make the facility more accessible to external customers and to align it with ISO/IEC 17025 standards, ensuring metrological traceability to SI units. These enhancements will enable the facility to participate in international proficiency testing and position it to achieve primary and accredited calibration provider status in the future. Together, these efforts address critical stakeholder needs while laying the foundation for continued advancements in heat flux measurement and calibration.

Calibration Facility & Methodology

Development of the calibration capability for high intensity heat flux sensors is an important portion of this project. Existing methods, procedures, hardware, and infrastructure was used to achieve the characterization of the flux sensors developed during this project. Building upon the existing knowledge and expertise at Sandia, the calibration process was refined, with additional quality control steps and improved uncertainty budget quantification. The procurement of a cavity radiometer, for use as a reference sensor, proved to be a challenge during the duration of this project. The project team pursued the steps required to become a traceable calibration entity, in collaboration with the Primary Standards Laboratory (PSL) at Sandia.

Facility and Capabilities

Hardware Upgrades

The NSTTF FGCF was outfitted with upgraded hardware to improve system operational effectiveness and improve overall efficiency of flux gauge characterization. The following items were added to the facility:

- FLIR IR camera
- Coolant digital flow meters
- Coolant pump upgrades
- All-sky camera
- Data acquisition modules
- Improved instrumentation
- Fixture equipment and hardware

A FLIR IR camera was added to the facility to enable real-time non-intrusive temperature measurement and monitoring of flux gauge sensing elements. This tool enables assessment of critical foil coating temperatures beyond which optical property change occurs, thereby nullifying the assigned characterization constant.

Digital coolant flow meters were installed to enable real-time measurement of system coolant flow rates. This was desired to provide higher confidence in coolant flow rates needed to maintain gauge and reference Kendall integrity, whilst also providing an applied coolant rate to abide by during gauge use.

Coolant pump upgrades were installed to provide higher cooling capacity capability for expanded testing in future projects

An all-sky camera was installed to improve operator experience, enabling real-time viewing of the sky and specifically cloud formation during characterization. This device improves operational efficiency.

Additional instrumentation and data logging equipment upgrades contribute to better quality control and quantification of the uncertainty of the traceable data logging chain.

Reference Sensor Traceability

The industry trade study highlighted the need for traceable measurements within the flux gage characterization process at the NSTTF FGCF. To enable future categorization of “calibration”, traceability was deemed a requirement. Several items were subject to establishment of traceability:

- Reference Kendall Radiometer calibration heater voltage measurement
- Reference Kendall Radiometer calibration heater resistance measurement
- Reference Kendall Radiometer flux aperture area
- Reference Kendall Radiometer control unit internal resistance
- Facility data acquisition voltage reader
- Facility data acquisition thermocouple voltage reader

Each item listed here was calibrated by the PSL at Sandia and returned to the NSTTF facility along with a traceable calibration certificate. These records are kept on file at the NSTTF.

Together, the traceable measurements established enable traceability for some aspects of the Kendall radiometer, but a complete traceable measurement could not be established for the self-calibration of the reference Kendall Radiometer utilized in flux gauge transfer characterizations. Aspects like the internal surface area, absorptivity/emissivity measurements of the internal coating of the cavity, reflectivity of the frontal silver coated face of the sensor, and the heat losses through the body of the sensor cannot practically be quantified to achieve a traceable measurement. The guidance from PSL is followed in establishing the traceability for the various parameters of the self-calibration for the Kendall radiometer.

Further, signal acquisition for the transfer calibration of a flux gauge relative to the reference sensor achieved traceable status via the traceably calibrated voltage and thermocouple data question cards. However, the term “characterization” is utilized rather than “calibration” in this report as ISO and PSL certification of technical “calibration” was not achieved within the period of performance of this project. Follow-on efforts will be conducted to obtain recognition of the NSTTF FGCF as a “calibration” entity.

Methodology

The NSTTF flux gauge characterization procedure was updated within this project, resulting in a proposed method for calibrating high-intensity heat flux gauges using concentrated solar light beyond limitations of existing ISO standards and accredited calibration bodies. The method establishes a relationship between the flux gauge voltage output and flux intensity through a two-stage process: evaluation and prediction. In the evaluation stage, the gauge to be calibrated and the reference sensor are exposed to 24 levels of heat flux. The range of heat flux investigated is determined by either the gauge's rating or the customer's desired testing range. Following this, the prediction stage employs an inverse weighted least squares (WLS) regression to establish a linear relationship between the gauge response and known flux levels. Additionally, this stage quantifies measurement uncertainties by considering systematic, statistical, and regression fitting errors. An abbreviated summary is presented herein, while further details will be available in our journal article, which is currently under review:

L. P. McLaughlin, L. G. Maldonado, H. Laubscher, B. Bean, J. Morrell, and K. Small, "A Proposed High-Intensity Heat Flux Gauge Calibration Method Using Concentrated Solar Radiation", Pending Acceptance, Journal of Solar Energy, May 2025.

The typical process for doing the heat flux characterization transfer from the reference sensor to the test sensor is described in the diagram below in Figure 1. The reference sensor and the test sensor are respectively exposed to the same concentrated solar flux source.

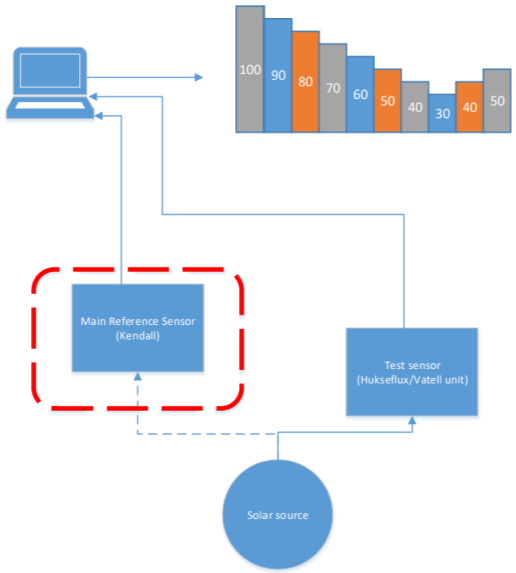

Figure 1: Flux sensor characterization transfer process

Traceable Calibration Status and Next Steps

The typical certification status for a calibration facility can be categorized in a few different levels. The scope of certification that was a stretch goal identified and pursued in this project is traceability. Given that obtaining any level of certification for a primary or secondary calibration facility can be a very time-consuming process, traceability status was identified to be the most relevant in this project. With the PSL at Sandia having an active ISO 17025 accredited status, the most feasible option would be to be affiliated with PSL and obtaining traceability for the measured parameters and all calibration hardware under the guidance and supervision of the PSL entity internal to Sandia. An illustration of the status of certification levels and the different stakeholders are given in Figure 2. The accredited calibration facilities for heat flux measurement are limited in the USA to the National Institute of Standards and Technology (NIST), with the European representation being the research Institute of Sweden (RISE), and the French Reference Laboratory Laboratory (LNE - Laboratoire national de métrologie et d'essais)

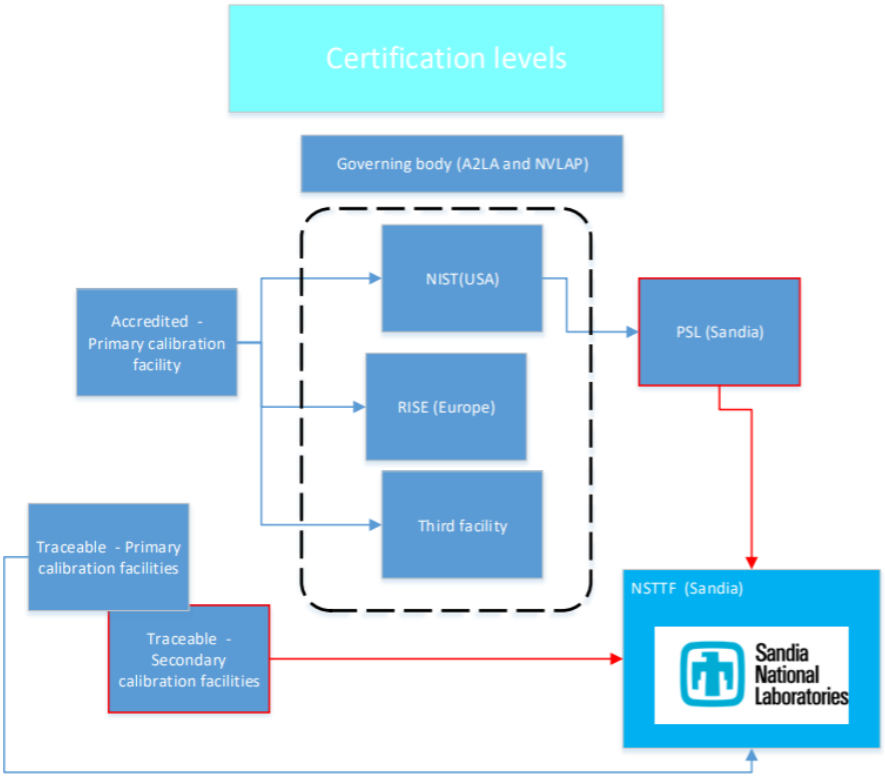

Figure 2: Certification levels and stakeholders in the calibration field

The NSTTF FGCF need to adhere to the following items to be able to obtain traceable status under the guidance of PSL as an extension of the calibration capability, referred to as an Accredited Calibration Partner (ACP) at Sandia.

Actionable items to become an APC at Sandia (Overseen by PSL):

1. Demonstrate traceable measurement of all the steps in the reference sensor calibration
2. Proof of calibrated hardware in accordance with ISO 17025 quality control processes

3. Provide uncertainty quantification for the full chain of data acquisition
4. Approved procedure of doing reference sensor calibration
5. Maintaining a trained person to operate the NSTTF FGCF
6. A Measurement Assurance Plan (MAP) for the calibration of the reference sensor and the transfer characterization of the test unit (sensor to be calibrated)
7. Maintaining the relationship and point of contact between NSTTF and PSL

The main challenge preventing full traceability status for high intensity flux levels (>1000 kW/m^2) at this point is the lack of a traceable reference sensor that can be used to verify fluxes in this range. Although a secondary transfer calibration can be achieved at the NSTTF FGCF with traceable reference back to NIST for up to 50 kW/m^2, this is still far below the range that the primary stakeholders require as per the trade study that was done in the beginning of the project. The cavity radiometer that is the state-of-the-art unit that had been historically used as the reference sensor in the transfer characterization process does not have a simple method of being calibrated in the flux ranges it can operate in. The current electrical heating/ electrical substitution self-calibration method is based on measurable parameters and a few assumptions for parameters that are not practical to measure. The main assumptions that are made based on the geometry and configuration layout of a cavity radiometer is that the absorption of the flux entering the cavity is >99.9%, based on internal re-radiation effects. The exact measurement of the absorptivity inside the cavity, the reflectivity from the frontal surface and the heat losses through the body of the cavity radiometer cannot practically be measured accurately.

As an alternative, identification of a blackbody calibration source and accompanying quantification method is the proposed next step for reference sensor calibration/verification with traceability back to basic IS units to close the circle on the reference sensor traceability measurement. Various methods are being discussed with PSL to enable a traceable flux source that can be used for the validation and comparison of the reference sensor to be used in the future for proceeding the calibration certification status.

1. Test Procedure

During the evaluation stage, the flux gauge to be characterized and the reference flux measurement device are exposed to 18 unique levels of concentrated solar flux, ranging from 20% to 110% of the gauge's nominal working range or the customer-requested range. Three exposure replicates are obtained at 20%, 50%, and 110% of the nominal gauge rating levels, resulting in a total of 24 flux exposures. This expanded number and variety of exposures align with ISO 19394-3 by achieving at least 10 unique flux levels during characterization. The acquired voltage signals from the gauge and reference sensor, along with thermocouple data, are utilized in the subsequent model fitting and uncertainty analysis, where recorded gauge voltages are correlated with known flux measurements.

The gauge and reference sensor exposure process involves the following steps:

1. Flux exposure levels are randomly assigned into one of four groups, each containing six increasing flux levels from a predefined list.

2. Measurements are initially recorded using the reference flux sensor for the six consecutive levels.

3. The test stand is repositioned, and gauge voltages are measured at the same six exposure levels.

4. The stage is repositioned once more, and measurements are again recorded using the reference flux sensor for the six consecutive levels.

5. Steps 2-4 are repeated for each group, resulting in a total of 24 measurements.

At flux levels below 3000 kW/m², a Kendall radiometer is utilized to determine the reference flux levels. This process is referred to as a secondary transfer process. The calibration of the Kendall radiometer itself is a primary transfer process, and this is achieved using traceable voltage, resistance, and aperture area measurements. Each of these measurements has been determined by the SNL Primary Standards Laboratory, and calibration certificates are kept on record. Gauge characterization with the Kendall radiometer offers high gauge prediction certainty due to minimal stages of uncertainty transfer.

2. Model Fitting and Uncertainty Quantification

The methodology for quantifying measurement uncertainties and fitting the characterization model for circular foil heat flux gauges was updated from prior NSTTF work and is described briefly here. Uncertainties are categorized into statistical (Type A) and systematic (Type B) components, combining them to determine the total measurement uncertainty. These uncertainties are then propagated through the model fitting process, which employs optimization to minimize the influence of measurement errors. Model fitting, voltage measurement, and flux measurement uncertainties are ultimately combined to determine expanded prediction uncertainty.

PSL did an uncertainty quantification of the measurement and characterization process, which is informed by all the input parameters from the team at the NSTTF.

Flux Gauge Development

Prototyping

Gauge prototyping efforts are summarized in detail in work published in the 2023 Solar PACES Conference Proceedings [2]. A summary is presented here.

1. Gauge Design Basis

The circular foil gauge, otherwise known as a Gardon gauge, was considered for development in this project given the outcomes of the industry trade study. A simple schematic of the circular foil gauge is shown in Figure 3. Circular foil gauges output a voltage response when exposed to heat flux, thus a relationship between known flux and gauge response can be established via calibration or characterization. Notably, the gauge sensing foil, which is typically made of constantan, is coated with an absorptive paint to create a well-defined radiation absorber over a broad wavelength range.

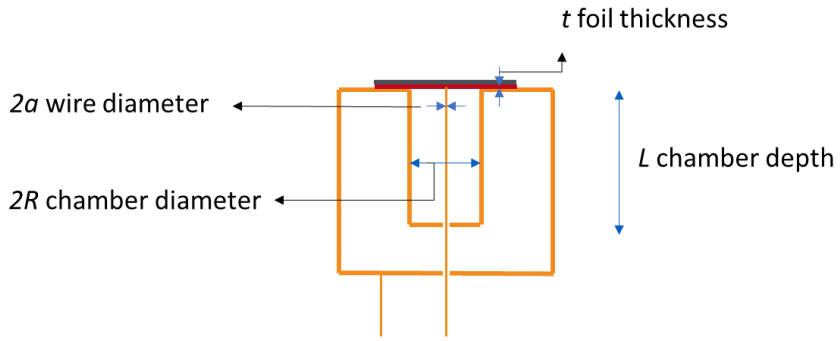

Figure 3. Circular foil gauge layout and dimensions directly influencing foil temperature.

2. Prototype Gauge Designs

Gauge foil temperatures can reach high temperatures at high flux levels, resulting in the change of coating properties like absorptance and emissivity. Thus, the relationship between incident flux and foil temperature is key to gauge design. Equation 1 describes a simplified flux-to-foil temperature relationship

$$T(r) = \frac{\Phi R^2}{4\lambda t}\left(1 - \left(\frac{r}{R}\right)^2\right) + T_C$$

where T is the foil temperature, Φ is the heat flux, R is the chamber diameter, r is the radial coordinate, λ is the thermal conductivity of the foil, t is the foil thickness and Tc is the cold junction temperature. To decrease the foil temperature and consequently the foil coating temperature, chamber diameter R can be decreased, or foil thickness can be increased.

Three prototype Gardon gauge designs were produced by Hukseflux and assessed in this work. Each design sought to decrease the foil coating temperature compared to existing commercial models. *To preserve the confidentiality of the project partner product specifications, generalized gauge design considerations are presented*. Table 1 lists each design name and design considerations. Five prototypes were produced for each gauge design, resulting in 15 prototype gauges available for testing in this study. Each gauge design utilizes an internal water-cooling loop to actively reject heat from the sensor.

Table 5. Prototype gauge design legend and generalized design considerations.

Name	Chamber Diameter	Foil Thickness
Model A	1 mm	200 µm
Model B	2 mm	200 µm
Model C	1 mm	100 µm
Model 0 (Baseline design)	2 mm	100 µm

3. Flux Gauge Characterization Method

Four of five prototypes of each gauge design were calibrated to 250 W/cm^2 at the NSTTF solar furnace or Flux Gauge Characterization Facility (FGCF) following a previously established NSTTF flux sensor characterization procedure [3]. This method was implemented as this work preceded method updates that resulted from this work. Flux gauges are exposed to concentrated solar flux at 20% (5x), 50% (2x), and 110% (5x) of gauges intended maximum operating level, totaling 12 solar flux exposures. Before and after each gauge exposure, the solar flux was measured with a Kendall Cavity Radiometer rated to 300 W/cm^2. An inverse regression was then performed to establish a linear relationship between the measured gauge response in millivolts and the measured heat flux level. Additional details regarding this method can be found in work by Mulholland et al. [3].

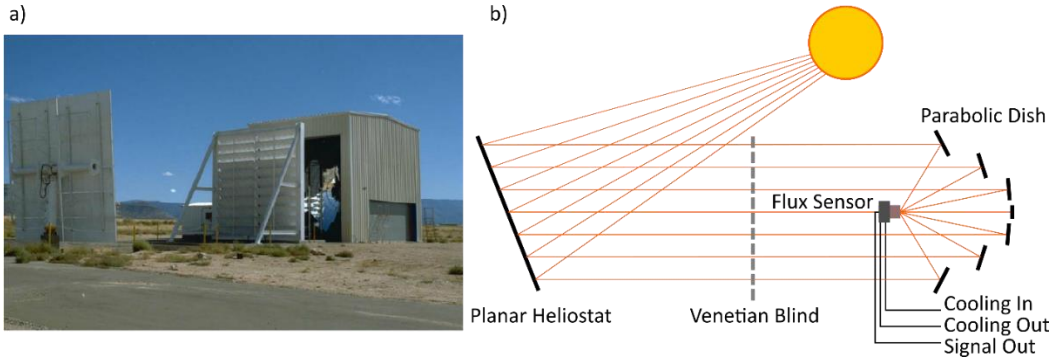

Figure 4. National Solar Thermal Test Facility (NSTTF) solar furnace facility. a) Solar furnace photograph and b) simplified working schematic.

A LabView data acquisition system was used to collect flux and temperature measurements during testing. A FLIR A-700 IR camera was used to non-intrusively measure the temperature of the flux gauge foil coatings during testing. A baseline foil coating emissivity measurement was set within the camera to enable an accurate temperature measurement ±2% according to the camera calibration. Each gauge was preconfigured with an internal thermocouple, and the gauge inlet & outlet coolant lines were instrumented with K-type thermocouples to enable real-time

temperature measurements. A suite of characterization results was produced for each gauge, including a regression summary table, characterization curve & residuals, foil coating temperature curve, and more. An example gauge characterization curve and residual plot are shown in Figure 5.

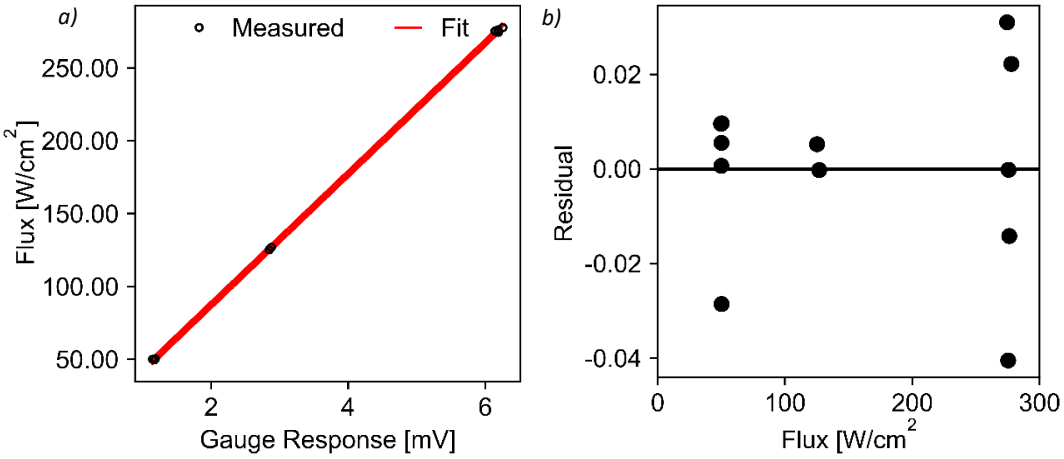

Figure 5. Example a) characterization curve and b) residual plot.

4. Rapid Exposure Testing

Rapid exposure testing was conducted following the characterization of flux gauges. The gauges were subjected to an intensity of 250 W/cm² for 100 cycles of 10 seconds each to evaluate how these exposure cycles affected measurement drift and uncertainty. Additionally, due to solar drift, the gauges were exposed to 250 W/cm² for 10 seconds across 10 consecutive shots. A baseline flux measurement was established both before and after the exposure of the gauges using the Kendall Radiometer. This entire procedure was repeated 10 times to complete a total of 100 exposure cycles. Two gauges from Model A and Model B designs were tested, along with one gauge from the Model C design. The testing was constrained by facility scheduling and the duration of the tests, limiting further experimentation.

Measurement uncertainty was analyzed to compare the accuracy of each gauge design and to quantify gauge drift over the 100 cycles. The overall measurement error for each gauge was evaluated as a combination of residual error, trial-to-trial error, and signal noise error. Each type of error—residual, trial-to-trial, and noise—was quantified. Measurements from the gauges and the Kendall Radiometer are indicated by superscripts ‘g’ and ‘k’, respectively, while time series measurements are denoted by subscript ‘i’. A total of twenty time series data points (n) were utilized to calculate time-averaged measurements, and up to one hundred trial measurements (m) were used for series-averaged measurements. Exposure cycles that encountered cloud cover or excessive wind were excluded from the analysis. In cases where multiple gauges of each design were tested, the combined errors were further aggregated using the square root of the sum of the squared combined errors.

$$u_{combined} = \sqrt{u_{noise}^2 + u_{residual}^2 + u_{trial}^2}$$

$$u_{noise} = \frac{\sqrt{\frac{1}{n-1}\sum_{i=1}^{n}\left(X_i^g - \overline{X^g}\right)^2}}{\overline{X^g}}, \overline{X^g} = \frac{1}{n}\sum_{i=1}^{n} X_i^g$$

$$u_{residual} = \frac{\overline{X^k} - \overline{X^g}}{\overline{X^k}}, \overline{X^k} = \frac{1}{n}\sum_{i=1}^{n} X_i^k$$

$$u_{trial} = \frac{\sqrt{\frac{1}{m-1}\sum_{i=1}^{m}(\overline{X^g} - \bar{X})^2}}{\bar{X}}, \bar{X} = \frac{1}{m}\sum_{i=1}^{m} \overline{X^g}$$

5. Overrated High Flux Testing

Overrated high flux testing was also performed at the NSTTF FGCF. One flux gauge from each prototype design was subjected to flux levels of 500 W/cm² or higher, surpassing the intended gauge rating of 250 W/cm². The purpose of this high flux exposure was to investigate trends in measurement error as flux levels increased and to identify potential failure mechanisms. A FLIR IR camera was utilized to monitor the temperature of the foil coating during each test, aiming to detect factors that could influence measurement error, including alterations in the optical properties of the foil coating. Prior to testing, the baseline coating emissivity was entered into the camera to ensure temperature readings were accurate within ± 2%, as specified by the manufacturer. This baseline emissivity was determined using a coated 25 mm x 25 mm constantan coupon. Due to the small size of the foil, coating emissivity measurements could not be obtained after degradation, so the emissivity was assumed to remain constant throughout all flux exposures. Consequently, any changes in coating emissivity resulting from high flux exposure would be reflected in temperature readings at a constant flux level.

The flux gauges were exposed to flux levels of 250, 300, 350, 400, 450, 500, and 550 W/cm² in sequential order. During testing, both the reference sensor and each gauge were actively cooled using internal cooling loops and were mounted in a water-cooled jacket. Measurement error was quantified following the methodology outlined in Section 2.3. The known flux was measured with the Kendall Radiometer up to 300 W/cm² and with a dedicated NSTTF high-intensity flux gauge up to 550 W/cm

6. Results

6.1 Flux Gauge Characterization

Twelve prototype gauges (4x of each design) were characterized in this campaign, and the derived sensitivity values are shown in Figure 6. Model A exhibited a broader spread of sensitivities across four protype gauges compared to Model B and Model C. Model A, which was designed to have the smaller chamber diameter and thicker foil, presented manufacturing challenges that may have attributed to the gauge-to-gauge variability in sensitivity. The sensitivities presented here were applied to their respective gauge to determine flux measurements in subsequent test campaigns.

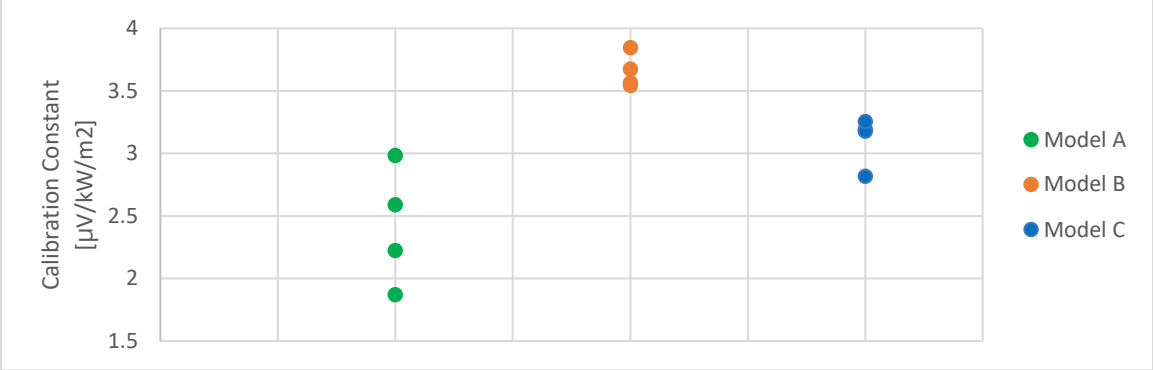

Figure 6: Prototype sensitivity results.

6.2 Rapid Exposure Testing

Two gauges of Models A & B and one gauge of Model C were exposed to 100x cycles of 250 W/cm^2. Figure 7 shows one cycle repeated 10x to obtain 100x total cycles. The errors described in Section 2 are reported in Table 2. The 100x cycle combined measurement error for each prototype was determined to be <5%. The noise and trial errors for each design were <0.15% and <2%, respectively. Residual error contributed the greatest to the combined error while remaining <4% for each design. Residual error in this context is a derivative of errors introduced from a non-perfect fit of the characterization regression. These results suggest that errors introduced from a non-perfect regression contribute the most to Gardon gauge measurement error, aligning with the findings of Guillot et. al for Vatell Gardon gauges [4].

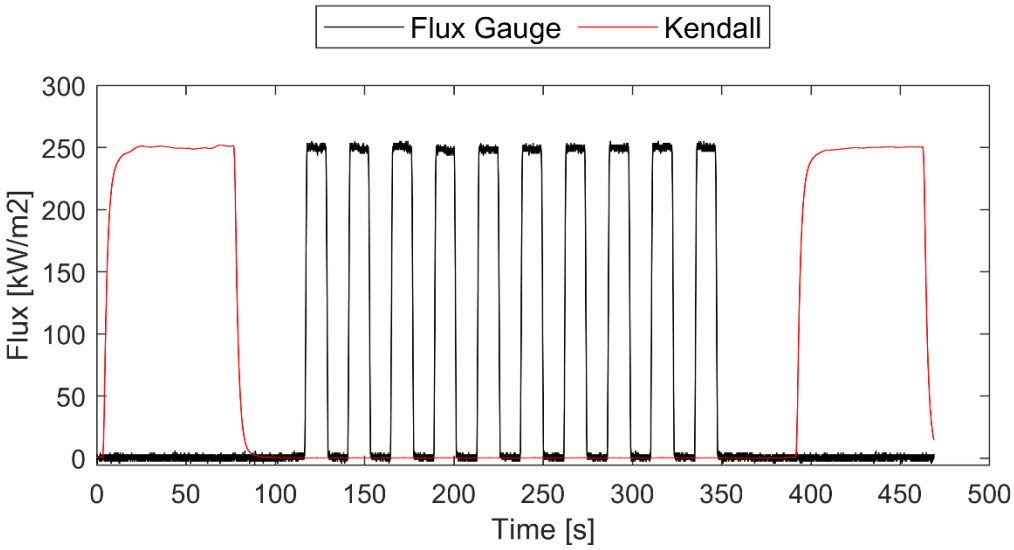

Figure 7: One of ten 10x rapid exposure cycles for Model A. 100x cycles were achieved in total. Baseline flux was determined before and after each 10x cycle.

The combined error was determined over the first and last 10x cycles to assess measurement drift during cyclic exposure. From the start to end of cycling, the combined error was found to slightly decrease, about 1%, for each gauge. The change in measurement error from the start to end of cycling may be attributed to a small change in the gauge response arising from changes in the physical and optical properties of the sensing element coating. In contrast, the 100x cycle combined error suggests that variability in test conditions throughout the entire test resulted in higher and lower errors at random periods in the 100x cycle period. Further testing is needed to conclude if gauge error drifted as a function of exposure cycles.

Table 6. Measurement error summary. Errors determined at 250 W/cm2 over 100x cycles.

Model	**% Noise**	**% Residual**	**% Trial**	**Combined % Error**	**First 10x Combined % Error**	**Last 10x Combined % Error**
Model A	0.13	2.85	1.91	3.43	2.04	1.25
Model B	0.09	3.94	1.78	4.32	3.24	1.99
Model C	0.14	3.05	1.10	3.25	2.26	1.74

6.3 High Flux Testing

6.3.1 Flux Measurement

One flux gauge of each prototype design was exposed to flux levels up to and >500 W/cm^2 to quantify key performance metrics at over-rated flux levels and to identify the degradation mechanisms of each design. Each prototype design physically survived the maximum capacity of the 16 kWt solar furnace facility (~600 W/cm^2). No weld failures, deformations of the gauge body, nor coolant loop failures were observed. It is noted that each gauge was internally cooled and mounted in a water-cooled jacket, contributing to the lack of gauge failure. Other gauge tests, not reported here, were used to iterate to a mount design that did not deform or cause gauge failure at high heat flux levels.

The flux measurement error as a function of true flux level is shown for each gauge design in Figure 8. The baseline flux measurement error of each prototype model was determined to be <4%. Measurement errors exceeding 5% occurred for Models B and C when exposed to targeted flux levels of 500 and 350 W/cm^2, respectively. The measurement error of Model A never exceeded 5%.

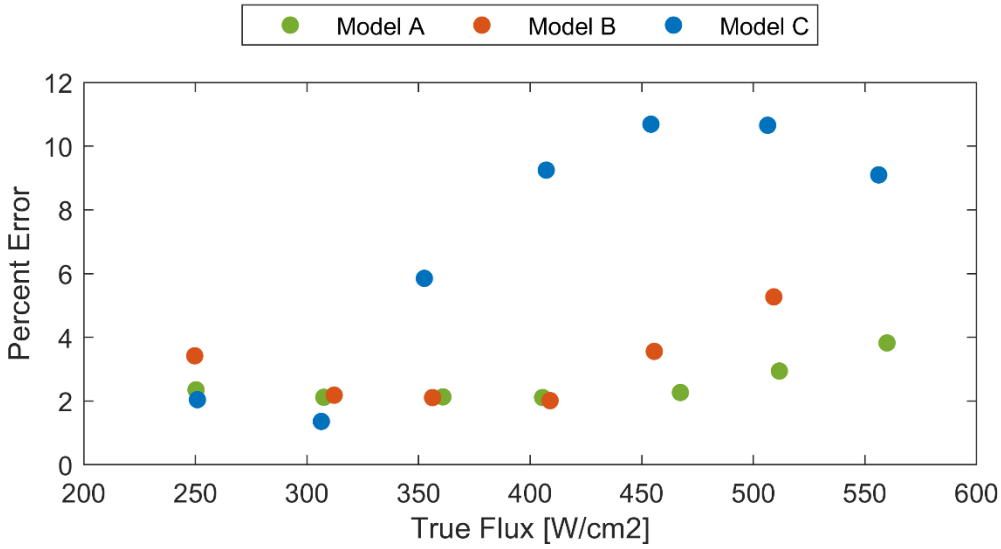

Figure 8: Measurement error vs flux level.

6.3.2 Coating Temperature

The peak flux gauge coating temperature as a function of reference flux level is shown in Figure 9. Peak coating temperature was determined as the maximum coating temperature measured during solar flux exposure. Model A exhibited the lowest peak coating temperature at each flux level. Model C peak coating temperatures were the highest at each flux level and Model B temperatures fell between Model A and C. A linear regression was applied to the peak temperature data over flux levels preceding an increased flux measurement error to elucidate trends pertaining to changes in coating optical properties and measurement error. Peak coating temperatures increased for all gauges at increasing flux level until 500 W/cm^2. This trend, however, was not linear over the full exposure range, suggesting that 1) the preset coating

emissivity decreased at increased flux levels and/or 2) the coating absorbed less energy as a result of decreased coating absorptance at increased flux levels. It was noted above that the measurement error of Models A, B, and C increased above the baseline 250 W/cm^2 error at flux levels of 500, 450, and 350 W/cm^2, respectively.

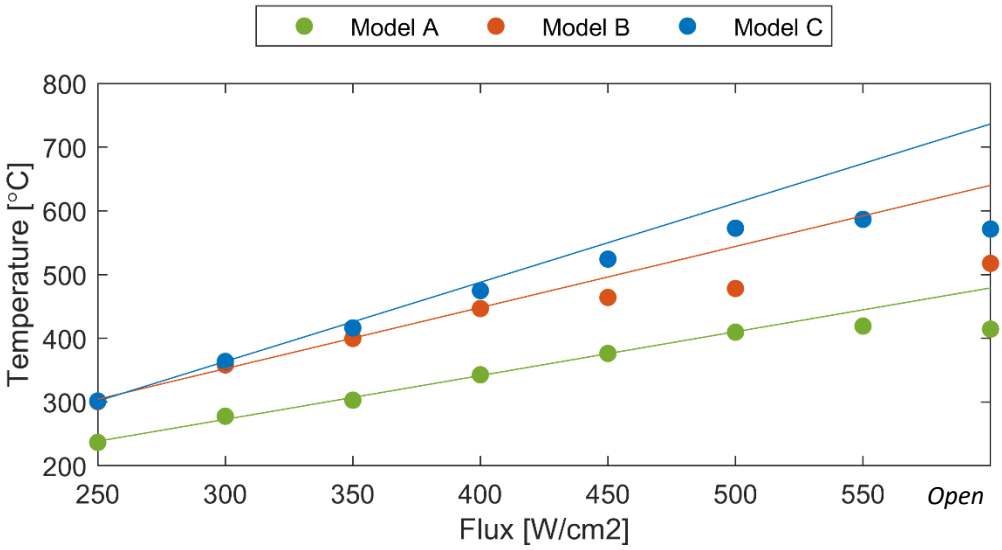

Figure 9: Peak coating temperature vs flux level.

These results suggest that the coating optical properties began gradually changing somewhere above 300 °C and before 400 °C. Rapid change occurred after coating temperatures met or exceeded 400 °C. Together coating temperature and measurement error results suggest that significant changes in coating optical properties occur near measured coating temperatures of 400 °C and result in a significant increase in measurement error. This analysis reveals a key finding of this study: Coating temperature, rather than flux level, largely dictates the maximum rating of the circular foil gauges assessed here.

Coating Assessment

Prototype testing revealed that coating degradation is the primary limitation of reliable Gardon gauge use at high heat flux. This finding prompted a comprehensive coating investigation which is presented in detail in [5]. A summary is presented here.

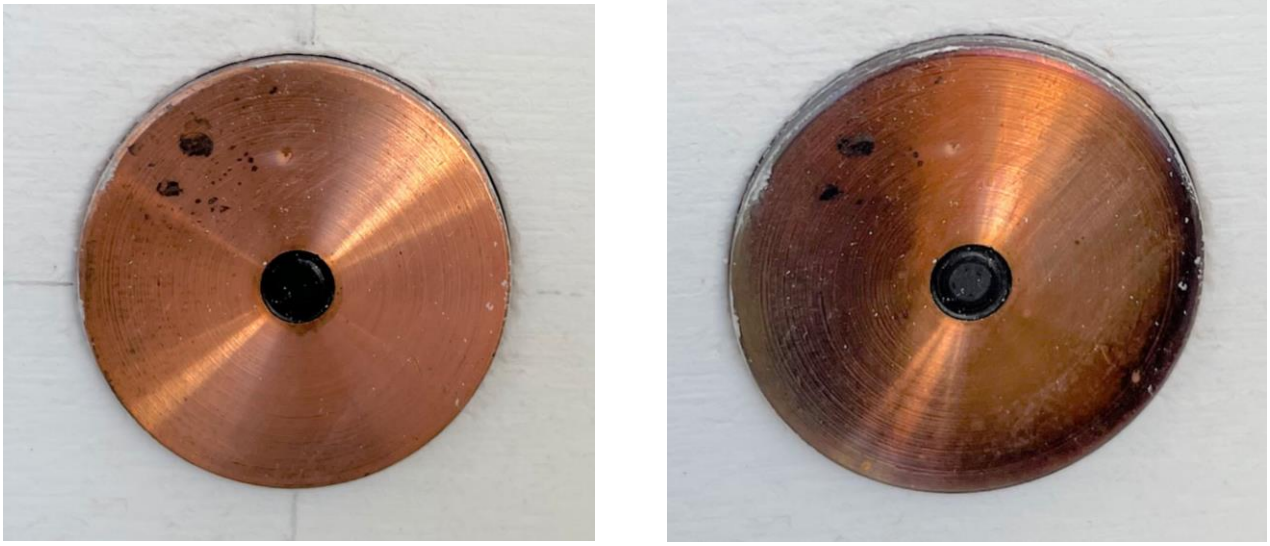

Figure 10. GG01 model coating degradation after exposure to 2500 kW/m2. Visual degradation/color alteration is observed.

1. Initial Coating Degradation Campaign

The durability of four high temperature coatings for use as a Gardon gauge foil coating were investigated given the large influence of foil coating on the flux level at which gauges can measure flux reliably. Four coating samples, listed in *Table 7*, were exposed to high flux solar simulator cycles and box furnace cycles, and optical property and physical degradation was quantified. Solar simulator tests assessed the impact of rapid solar flux cycles on degradation and the box furnace assessed the influence of prolonged high temperature exposure on degradation.

Table 7. Coating cost and maximum rated temperature. Short-hand coating names are shown in parentheses.

Coating	***Cost [$/gallon]***	***Maximum Temperature [°C]***	***Spray Method***
Rust-Oleum Hard Hat BBQ Black 7778 (RE)	*186.52*	*600*	*Can*
Rust-Oleum BBQ & Stove (RU)	*213.23*	*648*	*Can*
Pyromark 2500 (P)	*475.00*	*1093*	*Gun*
Solkote Hi-SORB-II (S)	*122.00*	*538*	*Gun*

Solar absorptance (α_s) and total hemispherical emittance (ε) were measured for each coating and combined into a single variable, referred to as the figure of merit (FOM) [6], to assess the stability of coating optical properties when exposed to high flux/temperature. The FOM is defined by the ratio of net radiative energy absorbed and retained by a coating to the net radiative energy absorbed and retained by an ideal absorber with absorptance of one and emittance of zero. Stability of the FOM directly relates to stability of flux measurement when utilizing a coated foil Gardon gauge for measurement. Equation 1 defines the FOM

$$FOM = \frac{\alpha_s Q - \varepsilon \sigma T_{max}^4}{Q}$$

where Q is the flux incident on the sample, T_{max} is the maximum surface temperature, and σ is the Stefan-Boltzmann constant. A flux of 10 W/cm^2 will be used for all FOM calculations in this work, and T_{max} is adjusted for each exposure scenario.

The physical state of each coating was qualitatively assessed before and after cycling using images taken with a Leica DMS1000 microscope. The microscope can capture images with a resolution up to 5 megapixels and up to 300x magnification. The camera exposure and imaging settings were kept constant to visually identify variation in the physical state of each coating.

Emissivity, absorptance, and FOM (Figure 11) remained nearly constant over 1000 solar simulator cycles for low and high temperature exposure scenarios. This finding was not anticipated as user experience suggests flux sensor foil coatings degrade after exposure to very high flux and temperatures. It is hypothesized that very brief exposure of coatings to high temperatures does not significantly degrade foil coatings. Per cycle during 550 °C testing, samples spent an average of 0.6 s exposed to temperatures over 500 °C, resulting in a total >500 °C exposure time of 10 minutes over 1000 cycles. The rapid heating, short total high temperature exposure time, and subsequent cooling of the sample between cycles did not demonstrate significant degradation on the coatings.

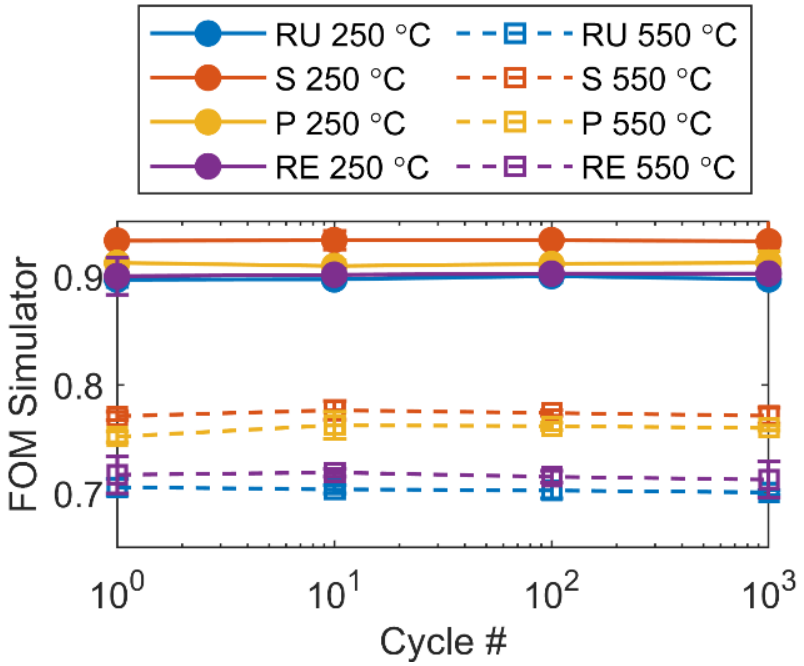

Figure 11. Figure of merit (FOM) as a function of solar simulator exposure cycles. Results are shown for cycles targeting peak surface temperatures of 250 °C and 550 °C. Near constant behavior observed.

In the box furnace tests, coating total hemispherical emissivity and solar absorptance were measured before and after exposure to 300, 400, and 500 C for 1-48 hours, and results were combined to determine the FOM (Figure 12). The optical properties of each coating remained nearly constant after 48 hours of exposure at 300 °C. At 400 °C, the RE and RU coatings showed degradation over the first 24 hrs. At 500 °C, each coating degraded after 1 hour of exposure. At both 400 °C and 500 °C, the coating properties are observed to stabilize after initial degradation.

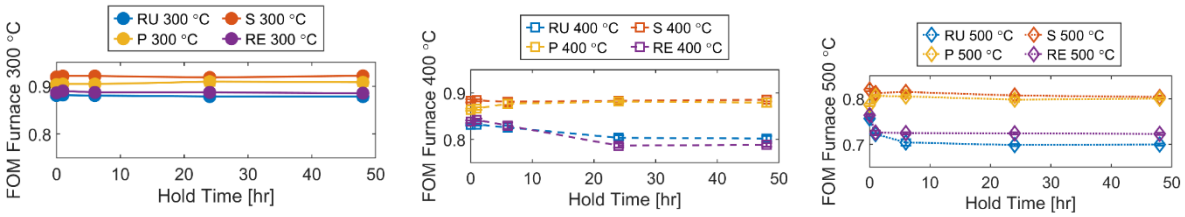

Figure 12. FOM as a function furnace hold time at pre-set temperatures of 300, 400, and 500 °C. FOM variation observed at temperatures ≥400 °C.

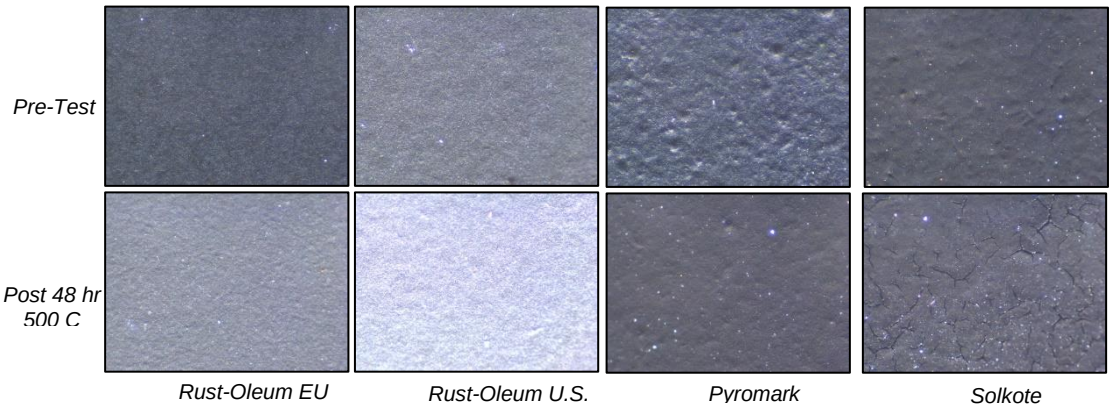

Figure 13. Microscope images of coatings before and after box furnace cycling

It was initially concluded that the combination of high temperatures and prolonged exposure provide the energy necessary to sustain coating surface reactions and alter optical and physical coating properties. Results also showed that coating properties stabilized after initial degradation due to prolonged high temperature exposure. This finding suggested that high temperature curing of flux sensor foil coatings prior to sensor characterization and use can increase the stability of flux sensor measurements in high flux and temperature applications at or below the curing temperature.

2. Inert vs Oxidative Coating Cure Assessment

The initial coating investigation identified pro-longed high temperature exposure as a means to stabilize flux gauge foil coatings. A follow-on assessment was conducted to assess the role of oxygen or oxidation on this process.

The HTS standard gauge coating, Rust-Oleum Hard Hat BBQ Black 7778, was tested for stability following an inert curing process prior to committing to an inert curing process for the final HTS flux sensor. The test was initiated due to a hypothesis that it is not high temperature alone that causes coating degradation, rather oxidation induced by high temperature environments.

2.1 Sample Preparation

To test the hypothesis, the following coated coupons were created:

A. 150 C cure in air (standard HTS process) – BASELINE
B. 500 C cure in air, 1-hr hold – OXIDATIVE HIGH TEMPERATURE (HT) CURE
C. 500 C cure in inert (N2) environment, 1-hr hold – INERT HT CURE (SHORT HOLD)
D. 500 C cure in inert (N2) environment, 2-hr hold – INERT HT CURE (LONG HOLD)

4x 25mm x 25 mm coupons were made for each process (A-D). 200 um thick constantan was utilized as the substrate – the same material used as the foil on the HTS Gardon gauge. Each

coating had an approximate coating thickness of 50 um. Following preparation, coatings were shipped from HTS to SNL for continued testing.

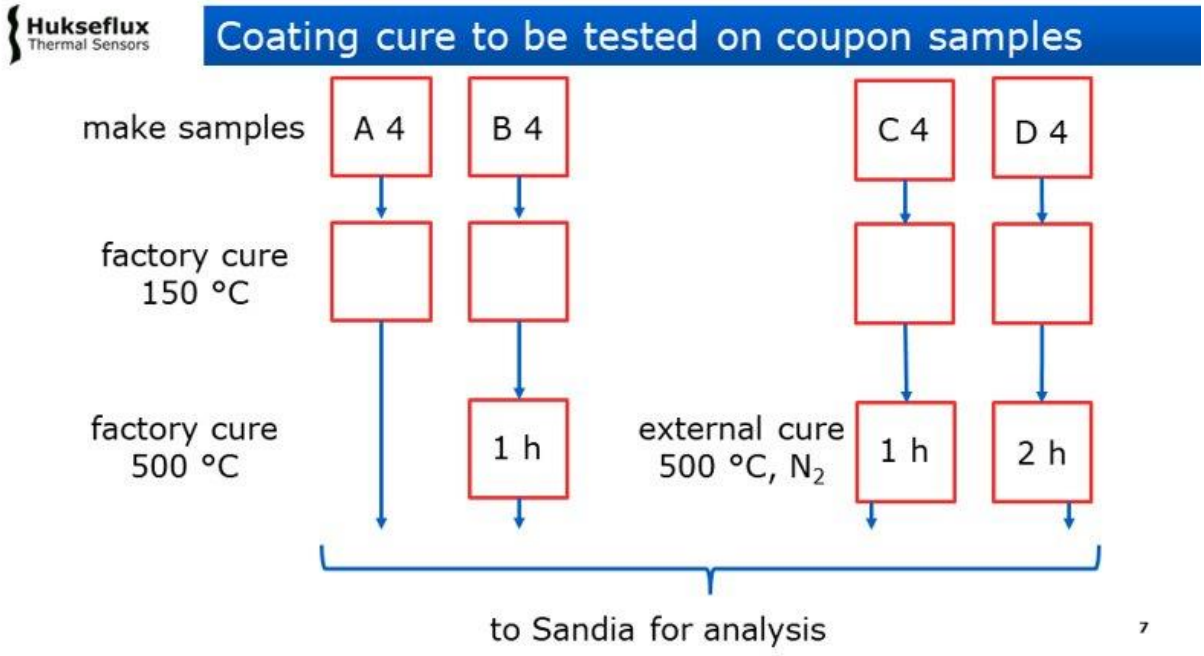

Figure 14. Coating coupon preparation methods A-D.

2.2 Optical Property Measurements

Solar absorptance (α_s) and hemispherical emittance (ε) were measured for each curing process to assess the stability of coating optical properties when exposed to temperature for prolonged durations. Spectrally resolved and integrated optical properties were determined, and both results sets are presented. A Surface Optics Corporation 410-0039 410Solar Reflectometer and 410-0038 ET100 Reflectometer were utilized for absorptance and emittance measurements, respectively. Three measurements were recorded for each optical property on the cycled sample before and after cycling, and measurement uncertainty was determined using Student's t-test with a 95% confidence interval.

2.3 Test Procedure

A high temperature box furnace (Sentro Tech Corp ST-1200C) was used heat and hold coated coupons at elevated temperatures for prolonged periods. The furnace utilizes an Eurotherm-3504 controller for temperature ramping, holding, and cooling control and is rated to 1200 °C. The furnace uses an exhaust chimney to vent hot gas during testing, and the furnace is lined with ceramic insulation. An integrated K-type thermocouple monitors environment temperature.

Coatings were held at temperatures of 300, 400, and 500 C for up to 6 hrs. Unique coupons were used for 300, 400, and 500 C experiments to ensure impacts of further curing did not influence the observed trends. Coupons were ramped to the desired temperature at 5 C/min and held isothermal. Coating optical properties were measured after 0, 0.5, 1, 2, 4 , and 6 hrs of holding. Note: 300C and 500 C 6 hr data points were not finished at the time this report was created.

2.4 Results

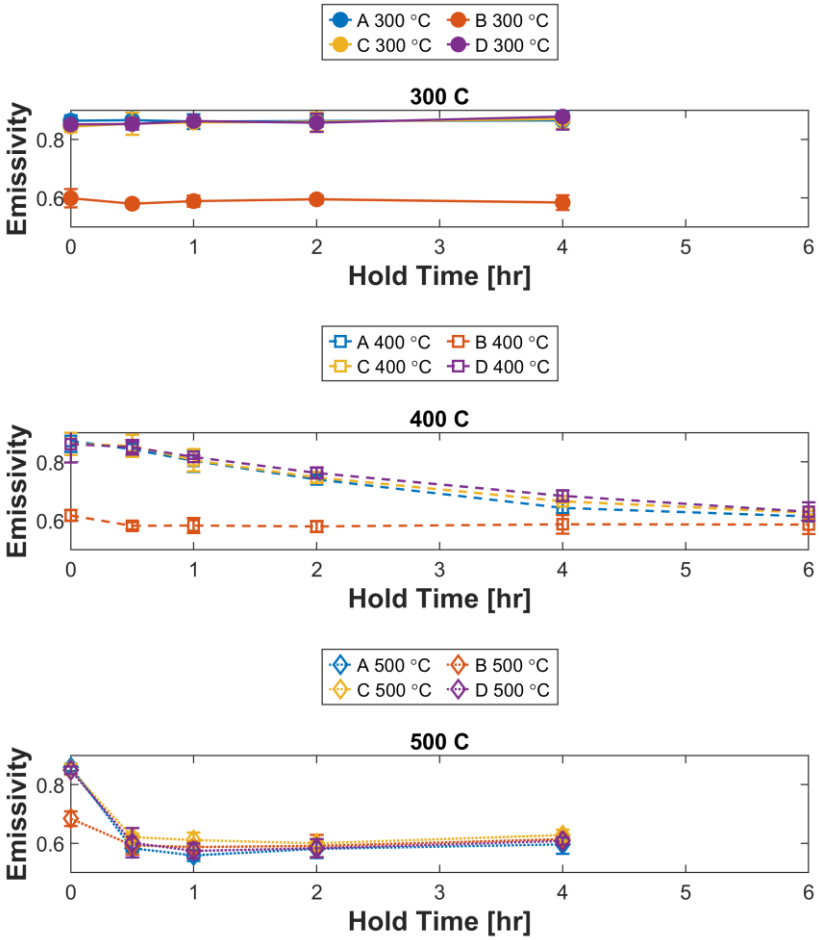

Figure 15. Total hemispherical emissivity as a function of hold time and furnace temperature for each sample type (A-D).

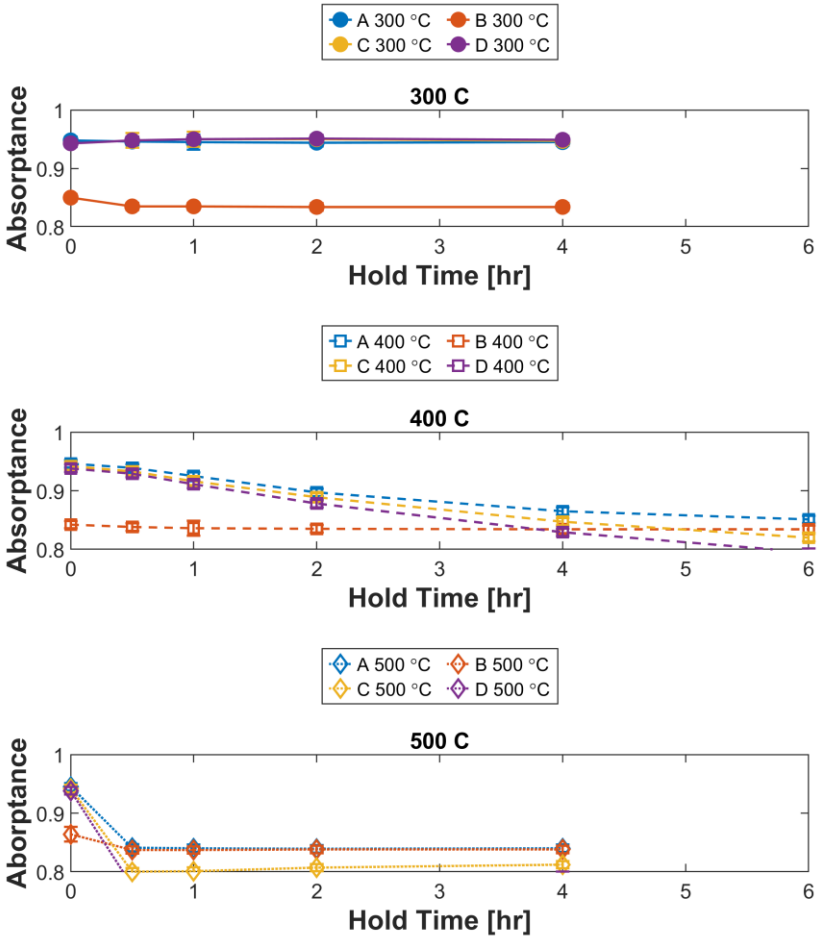

Figure 16. Total absorptance as a function of hold time and furnace temperature for each sample type (A-D).

The optical properties of each coating sample (A-D) are observed to be constant over 6 hrs at a furnace temperature of 300 °C, as shown in Figure 15 and Figure 16. Notably, sample B has a lower total hemispherical emissivity and total absorptance than Samples A, C, and D, and this result is due to the optical degradation induced by the 500 C oxidative cure prior to testing in this campaign. Samples A, C, and D experienced gradual and rapid decreases of emissivity and absorptivity over 6 hrs of exposure to 400 °C and 500 °C, respectively. Sample B optical properties remained constant from 0-6 hr at 400 °C while the Sample B optical properties slightly decreased over the first 0.5 hr exposure at 500 °C before remaining constant from 0.5-6 hr. The optical properties of each sample converged after 4 hrs at 400 °C while the optical properties of each sample converged and became constant after 0.5 hrs at 500 °C. The optical properties of Samples A, C, and D converged with that of sample B in both 400 °C and 500 °C environments. This result suggests that the extent of coating degradation is not solely a product of temperature, rather a product of temperature & time, or energy.

The results show that the samples cured in an inert environment at 500 °C (C & D) showed no additional resistance to degradation in high temperature oxidative environments (400 °C and 500 °C) compared to the 150 °C oxidative standard curing process (A). Samples A, C, and D degraded at the same rate and converged at the same absolute optical properties in the 400 °C and 500 °C environments. The results confirms the hypothesis that the Rust-Oleum optical degradation is not simply a product of high temperature but the product of surface oxidation induced by high temperatures in an oxidative environment.

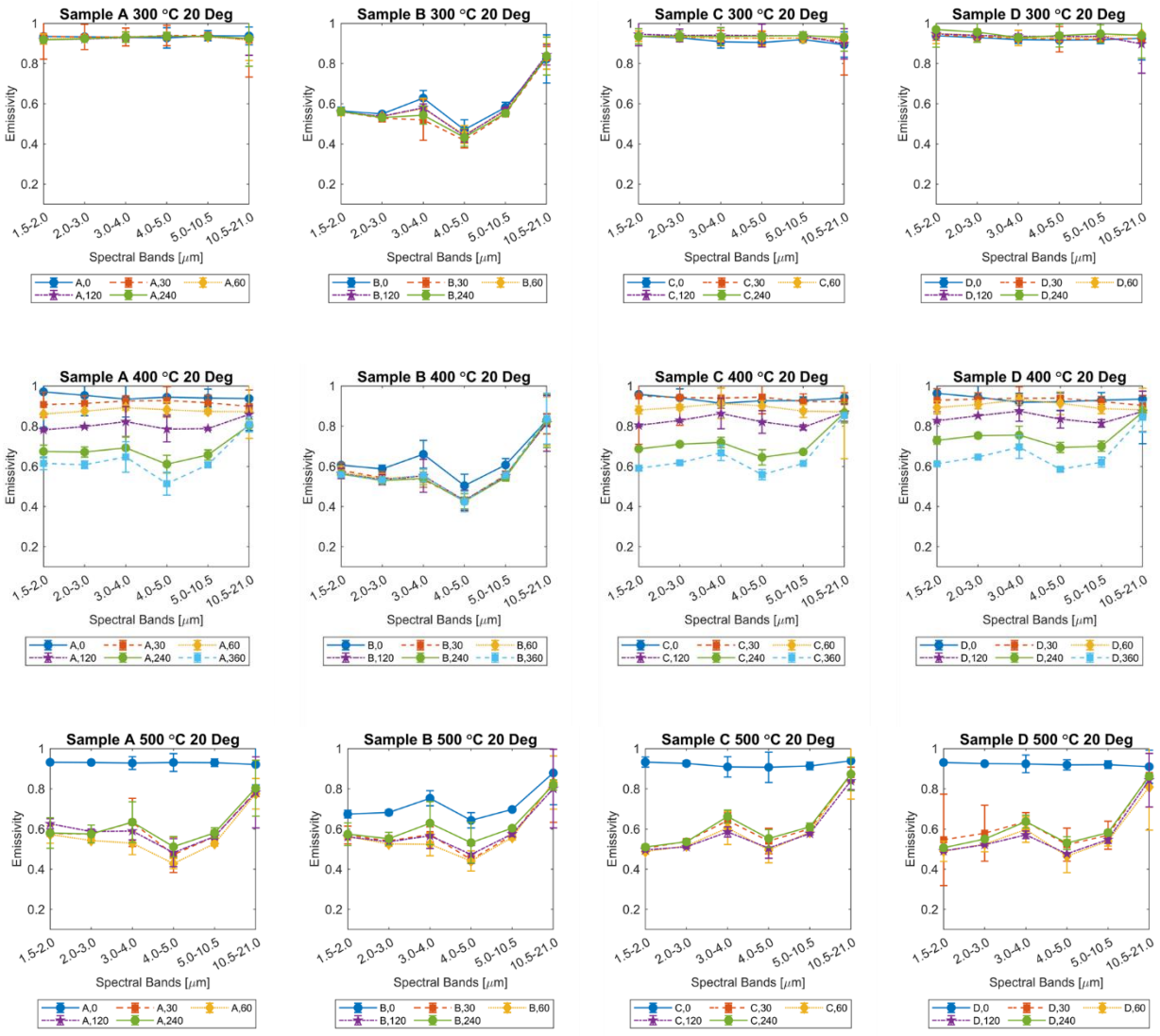

Figure 17. Spectrally resolved emissivity of each coating sample (A-D) after increased exposure to 300 °C (top), 400 °C (middle), and 500 °C (bottom). Results for 20-degree specular angle shown. Legend Key: Sample,Hold_Duration (e.g. A,30 = Sample A after 30 minute hold)

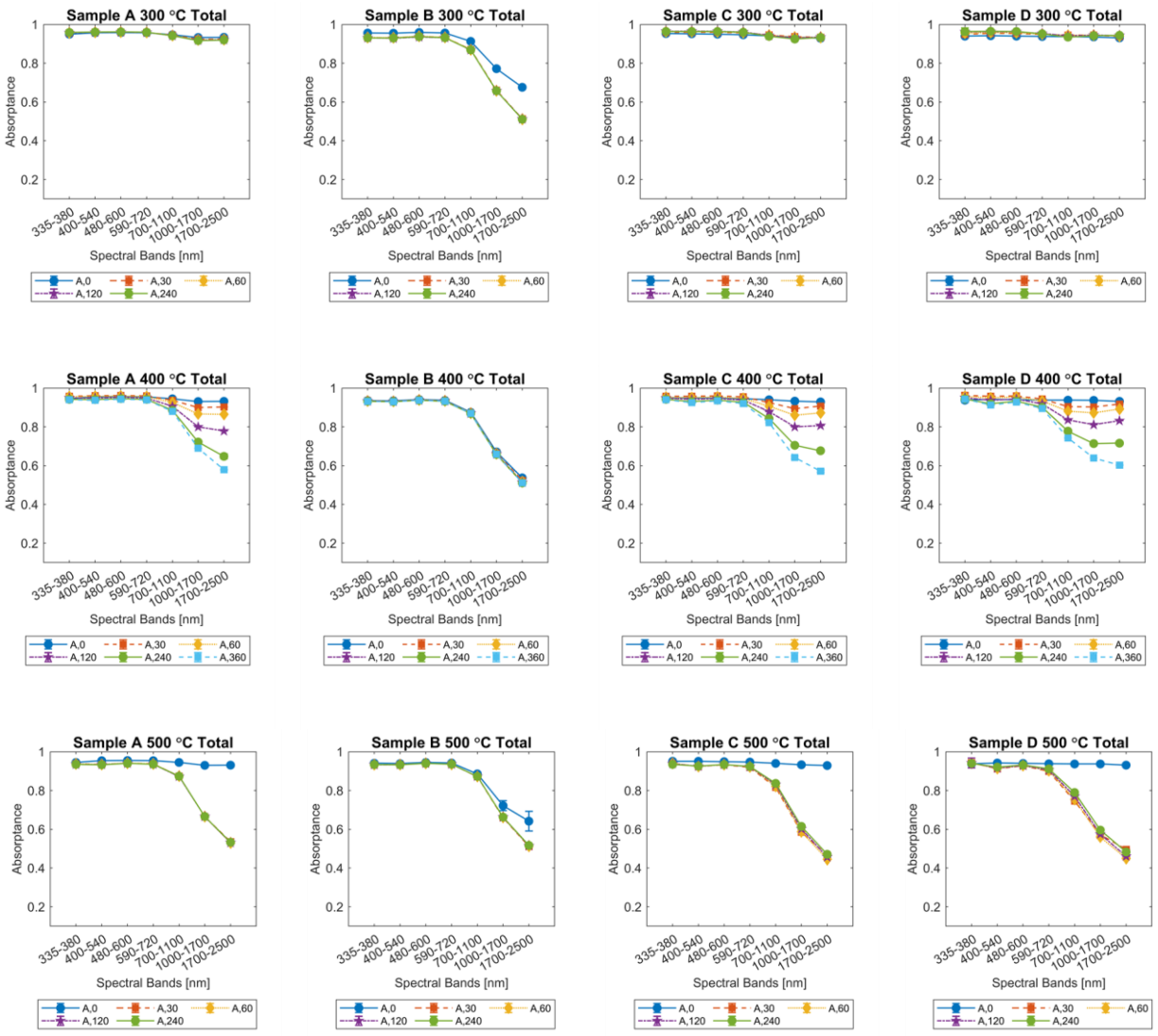

Figure 18. Spectrally resolved absorptivity of each coating sample (A-D) after increased exposure to 300 °C (top), 400 °C (middle), and 500 °C (bottom). Legend Key: Sample, Hold, Duration (e.g. A,30 = Sample A after 30 minute hold)

Spectrally resolved data, shown in Figure 17 and Figure 18, supports the integrated results discussed above. Rapid optical property degradation occurred in the 500 °C environment, gradual degradation occurred in the 400 °C environment, and no degradation occurred in the 300 °C environment.

Further, the results reveal that optical degradation occurs in specific spectral bands rather than uniformly across the spectrum. Emissivity notably decreased with increased high temperature exposure between 1.5-10.5 um (Note: minimum emissivity spectral band = 1.5 um). Absorptance decreased significantly at spectral wavelengths above ~700 nm while nearly no degradation

occurred below ~700 nm. This result importantly reveals that high temperature oxidative coating curing, although effective at creating a stable coating, creates non-uniform absorptance and emittance profiles. Gardon gauge physics rely on a spectrally flat absorption and emission profile to provide an accurate measurement across a full spectral range of incident radiation (radiative heat flux). The non-unform spectral coating profiles here imply that a Gardon gauge with a 500 °C oxidative coating cure will provide different measurement results for the same heat flux level when the radiation source is in the UV-Vis spectral range and the IR range.

Together, the total and spectrally resolved results imply the following

1. Rust-Oleum Hard Hat BBQ Black 7778 degradation is a product of surface oxidation caused by high temperatures (>300 °C) in an oxidative environment
2. High temperature inert curing does not stabilize coating optical properties for high temperature measurements in oxidative environments
3. High temperature oxidative curing induces stable but non-uniform absorption and emittance profiles that a) limit the measurement use of the Gardon gauge to specific spectral bands or b) require multiple characterizations to capture performance in multiple spectral bands

Gauge & Coating Down Selection

The Model A gauge design was shown to maintain a constant measurement error up to 450 W/cm2 while the Model B design showed an initial decrease in measurement error following exposure to 300 W/cm2 before stabilizing until exposure to 450 W/cm2. For both models, a coating temperature > 300 °C induced the observed changes in measurement error. Despite the 1.5x200 variant superior stability, the model originally posed manufacturing challenges, requires new gauge housings and unique parts compared to the standard GG01-100 product, and a has a sensitivity nearly 66% that of the 2x200 variant. The Model B design utilizes the same hardware as existing HTS products, is easy to make, and has the highest sensitivity. Given the manufacturing challenges and benefits associated with Model A and Model B designs, respectively, the decision was made to proceed with Model B as the final product design.

Coating assessments demonstrated that high temperature and oxidative curing is beneficial to coating stability. Despite the benefits, it was determined that the standard HTS curing process was suitable for a heat flux gauge rated for 250 W/cm2. Higher temperature curing posed manufacturing difficulty and added cost. Given these realities, the standard cure was pursued. Furthermore, the standard HTS coating showed the greatest stability at lower temperature curing, as compared to Pyromark and Solkote, therefore the standard HTS Rust-Oleum coating was selected for the final product.

Additional Design Improvements

Early product testing revealed a critical vulnerability in the heat flux gauge design: high flux exposure, especially to the side walls, induced mechanical stresses on the internal cooling loop

welds, leading to, catastrophic failures during extreme high flux conditions. An image of a failed gauge, along with scanning electron microscopy (SEM) evidence of weld failure, is presented below in Figure 19 and Figure 20. In response to this finding, HTS relocated the coolant chamber weld from the front surface of the gauge to a position further down the gauge body, thereby reducing the thermal stress on the welds and enhancing the overall durability of the design.

Figure 19. Failed gauge due to side wall heating.

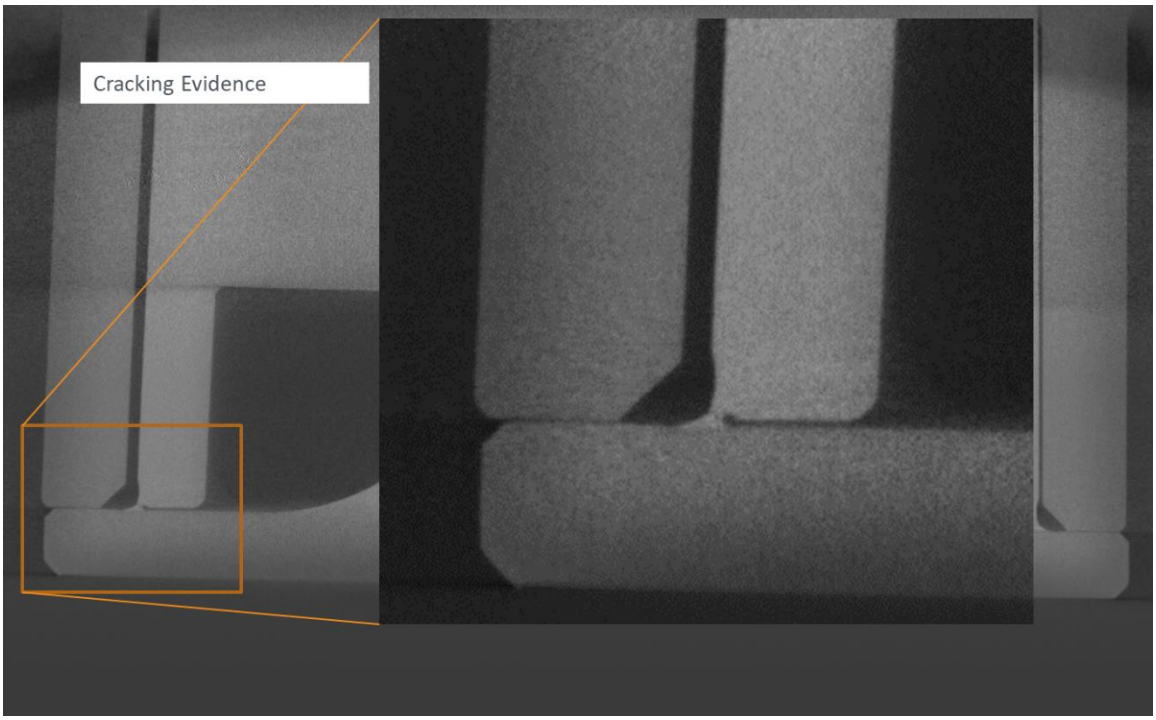

Figure 20. SEM images showing weld failure.

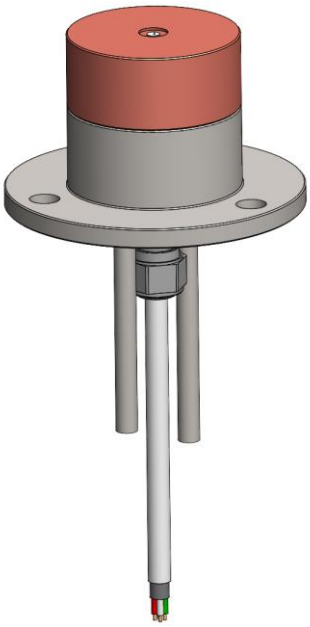

Figure 21. Updated gauge coolant weld location (Weld location distanced from front surface).

Another significant design enhancement involves the transition to a two-part assembly for the entire gauge. The first assembly consists of a the copper body, while the second assembly features a stainless steel shield that houses the circuitry and other sensitive wiring components. This modular design not only improves thermal management but also facilitates high-temperature curing of coatings in future iterations, should the market demand higher-rated flux products.

To further bolster the gauge's robustness against high temperatures, HTS implemented several additional improvements, particularly concerning the internal circuitry and interfaces. These enhancements include:

1. **Improved Foil Overlap and Welding Technique:** HTS refined the welding technique for the constantan foil to the copper body, ensuring a more reliable and consistent electrical connection that can withstand high thermal loads.
2. **Pressure Fit Inlet/Outlet Coolant Tubing:** The coolant tubing is now designed with a pressure fit mechanism, enhancing the integrity of the coolant flow and reducing the risk of leaks under high-pressure conditions.
3. **Ceramic PCB for Signal Processing:** HTS integrated a ceramic printed circuit board (PCB) for signal processing, which offers superior thermal stability and reliability compared to traditional materials, ensuring consistent performance in extreme conditions.
4. **Clamped Signal Wire:** The signal wire is now secured with a clamping mechanism, minimizing the risk of disconnection or damage during operation.
5. **Cable Gland Insert:** A cable gland has been added to replace the clamped wire connection, to allow the instrument to be more easily serviced.

Because in the final product, there is no need to perform the on-gauge curing at high temperature, the improvements listed under bullet 2,3 and 4 above are not included in the final design, as they would add unnecessary costs without adding value.

These designs have been tested, and are available for use in future product developments

Final Product Testing & Validation

The NSTTF team received five gauges of the final design from HTS with the task of properly characterizing their performance. The objectives included characterizing gauge response, identifying the maximum exposure levels before characterization invalidation occurs, assessing the impact of coolant flow rate and temperature on performance, evaluating the gauges' ability to withstand prolonged exposure, and examining how coating thickness influences resistance to degradation under high flux conditions.

1. Flux Gauge Characterization

The first test campaign focused on executing accurate characterization of the gauges sensitivity, seeking repeatable and reliable results. The process and a summary of its execution are described in the ***Characterization Facility and Methodology – Testing Procedure*** section earlier in this report.

Figure 22 shows an example characterization result from this campaign. This result was derived by relating the gauge response to flux levels given by the Kendall radiometer (secondary transfer process). Flux prediction uncertainty reflects uncertainty in model fitting, measurement error, and systematic error. Expanded measurement uncertainty (95% CI) determined for the gauges evaluated were determined to have uncertainty ranging ± 5-12.5 W/cm^2 or 2-5% at 250 W/ cm^2. This result aligned with an initial project goal of achieving a 250 W/cm^2 gauge with uncertainty <5%.

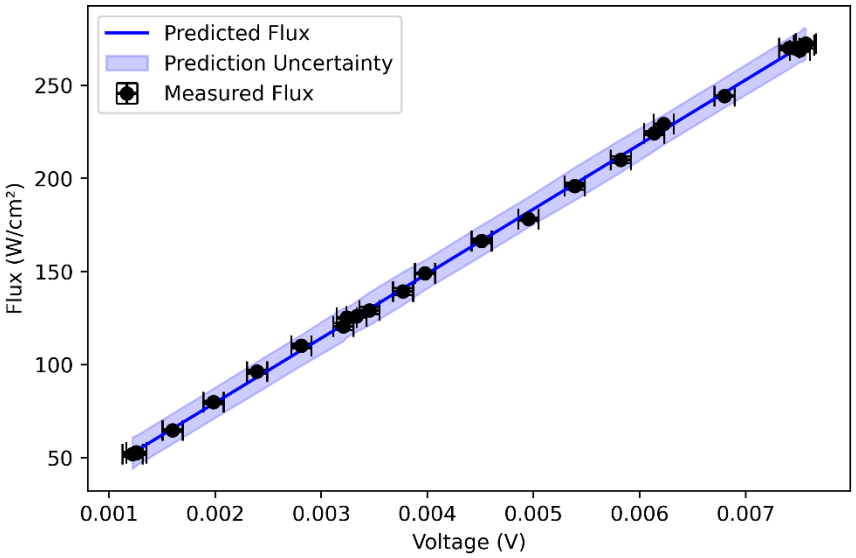

Figure 22. Example characterization with 95% confidence interval uncertainty limits.

Figure 23 provides a breakdown of the uncertainty contributions. It is evident that the uncertainty from gauge voltage measurements is the largest contributor to the total expanded uncertainty. Notably, the gauge voltage uncertainty is >95% systematic error associated with the FGCF data acquisition cards. The remaining contributions to the total expanded uncertainty come from model fit and flux measurement errors associated with the reference Kendall radiometer.

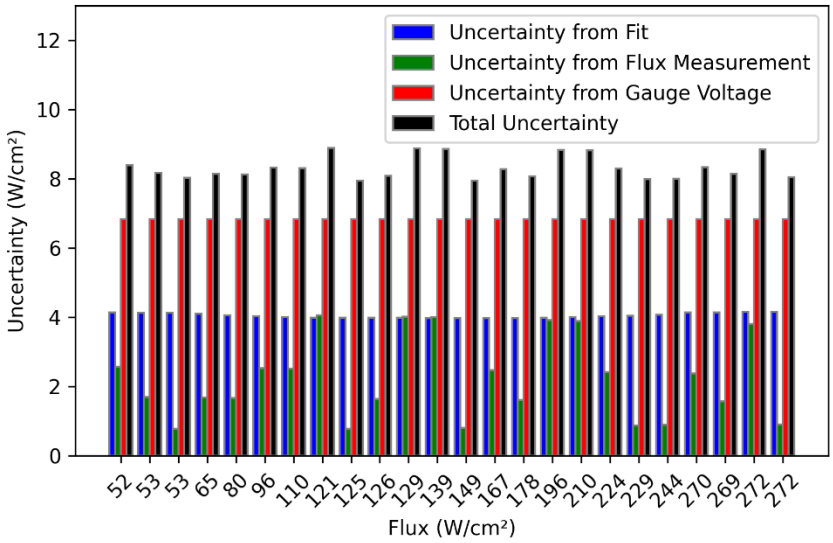

Figure 23. Flux prediction uncertainty breakdown.

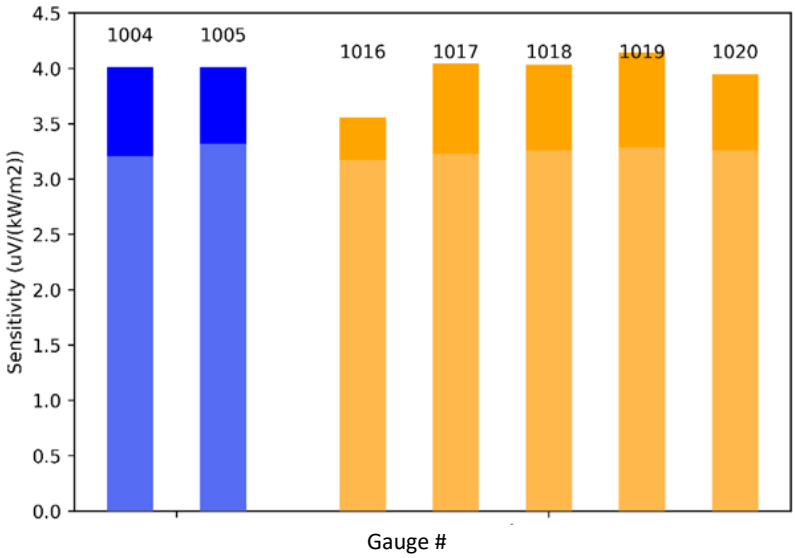

Figure 24. *Sensitivity of all* 5 final product gauges (yellow) compared to prototype gauges of the same design (blue)

Figure 24 compares the Hukseflux calculated gauge sensitivity to the NSTTF's characterized gauge sensitivity for final product gauges as well as prototype gauges of the same design. Gauges were shown to have repeatable sensitives in both the HTS and SNL characterization sets. Gauge sensitivities varied <1% for six of the seven gauges evaluated, while one gauge exhibited some outlier behavior. In total the gauge sensitives ranged from 3.5 to 4.1 µV/kW/m^2. Final gauge products were also shown to compare very well to prototype products of the same design. This finding provides confidence that gauge fabrication and the SNL & HTS characterization processes are repeatable and reliable within a 85% confidence rate.

The sensitivity of the NSTTF heat flux gauge consistently exceeded the estimates provided by Hukseflux by approximately 0.5 to 075 µV/kW/m², a trend that was consistently observed throughout the project. This discrepancy is hypothesized to stem from a slight non-linearity in the gauge's response at lower flux levels. HTS is only able to characterize gauges with multiple points up to 10 W/cm^2 and a single data point at 100 W/cm^2. This majority of HTS characterization points used to determine their reported sensitivity value are much lower than those used to characterize the gauge at the FGCF at the NSTTF. As illustrated in Figure 25, the sensitivity of the gauge was measured to be lower at lower flux levels, aligning with the discrepancy observed between SNL and HTS derived sensitives.

For the developed product, this issue is solved by implementing a transfer standard in the factory calibration process that is characterized at Sandia over the (100 - 300) W/cm² flux range.

The observed trend indicates that the gauge's sensitivity diminishes at lower flux levels, while it remains stable and consistent at higher flux levels. Ideally, one would expect the gauge to exhibit perfect linearity across an infinite range; however, practical fabrication and testing conditions can introduce variations that affect this ideal performance. Consequently, our findings suggest that the final product, rated for 250 W/cm², is best utilized within a flux range of approximately

100 W/cm² to 250 W/cm². For measurements at lower flux levels, it is advisable to employ a gauge specifically designed for that range, such as the existing 100 W/cm² rated Gardon gauges, which would provide more accurate readings in those conditions. This understanding is crucial for optimizing the application of the 250 W/cm2 gauge and ensuring reliable measurements across varying operational scenarios.

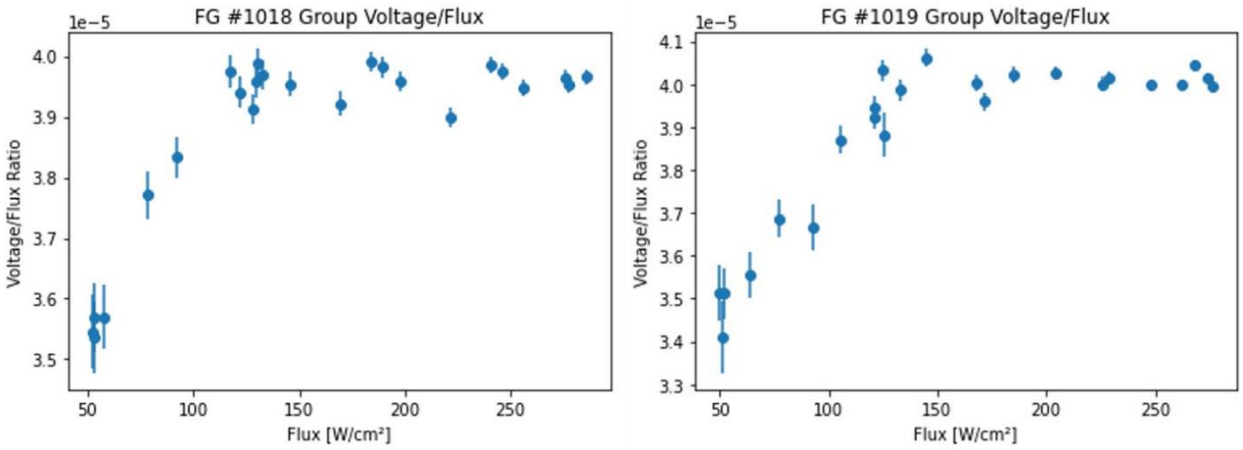

Figure 25. *Voltage-to-Flux ratio (i.e. sensitivity) as function of flux level.*

2. Overrated High Flux Testing

The second test campaign focused on evaluating the effects of exposing the gauges to flux levels that exceeded their designed rating. The primary objectives of this testing were to verify that the final product is suitable for measurement up to a rating of 250 W/cm2 and determine the flux level beyond which measurements are no longer reliable. Further, the testing sought additional insights regarding the impact of high heat flux on coating degradation and ability of the heat flux gauge to withstand high energy fluxes. The methodology for conducting overrated high flux testing here matches that of the ***Prototyping - 6.3*** section.

Figure 26 shows the percent error of the HTS gauge when measuring 250 W/cm2 as compared to the Kendall radiometer after exposure to increasing flux levels. Results are shown for two final product gauges (1019, 1020) and two prototype gauges having the final product configuration (1004, 1005). The results shows that the percent error of the baseline 250 W/cm2 increased 1% above the pre-high flux exposure error consistently near 400-450 W/cm2. The result consequently shows that the baseline measurement error remained constant or even decreased between 250-400 W/cm2. This finding confirms that the final HTS product is suitable for 250 W/cm2 operations, with an additional margin of 150% prior to significant increase in measurement error.

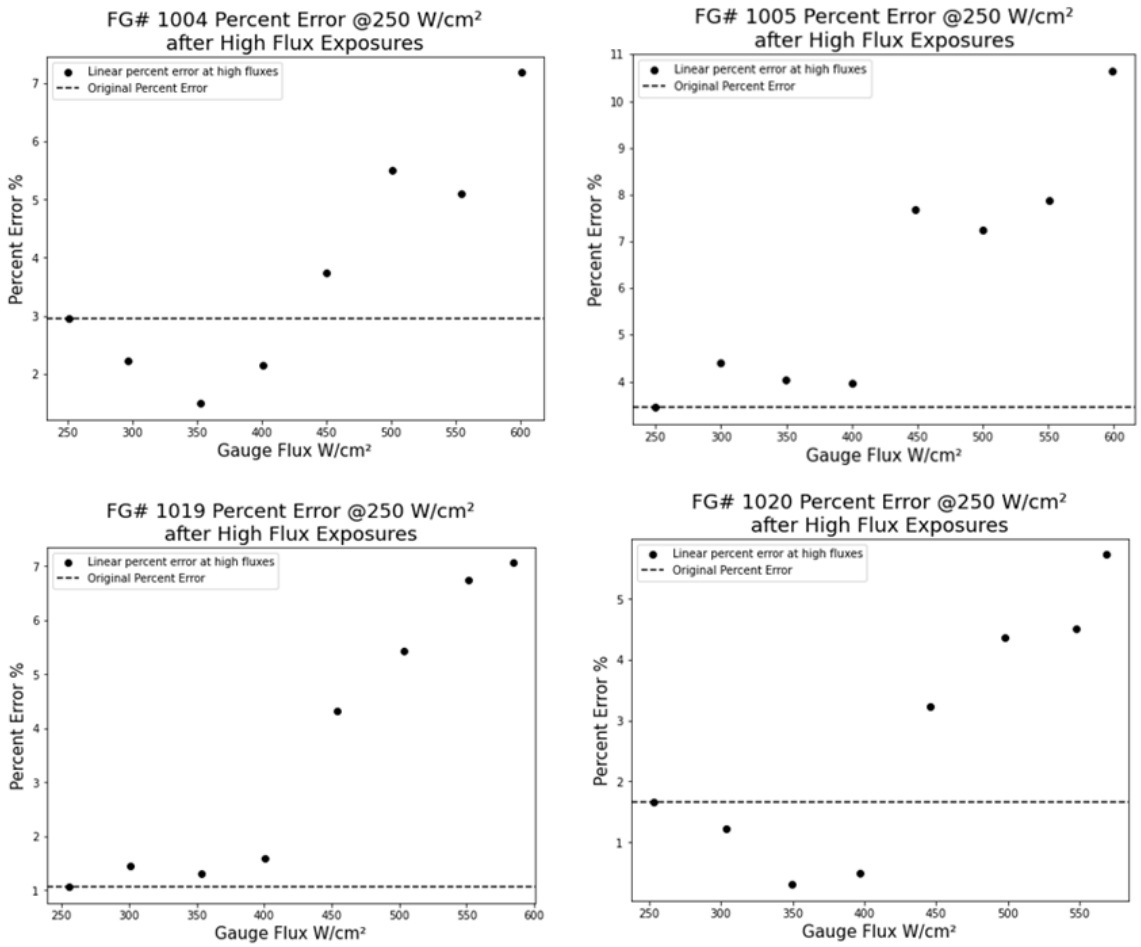

Figure 26. Measurement error as a function of flux level.

3. Coolant Flow Rate and Temperature

The third test campaign was dedicated to investigating the effects of varying coolant temperatures and coolant flow rates on gauge performance. During baseline characterization, the coolant temperature and flow rate were maintained at constant values of 32°F and 0.3 gpm, respectively. First, the baseline coolant flow rate of 0.3 gpm was assessed at four different coolant temperatures: 32°F, 45°F, 60°F, and 75°F. During this phase, both the Kendall radiometer and the gauge were sequentially exposed to flux levels of 50, 125, and 275 W/cm². This testing procedure was repeated for each coolant temperature. Subsequently, we conducted the same tests using a coolant flow rate of 0.1 gpm, again for each coolant temperature, and ensuring that the Kendall's coolant flow rate remained at its baseline value to prevent any potential damage to the instrument. For each combination of flux level, coolant temperature, and coolant flow rate, we calculated the relative error of the gauge compared to the readings from the Kendall radiometer.

The results indicated that neither coolant temperature nor flow rate significantly affected gauge performance, as results exhibit no clear trend in measurement error vs coolant temperature or flow rate. Figure 27 and Figure 28 illustrate the comparisons of gauge behavior across the different test runs, confirming that the applied variations in coolant conditions did not have a meaningful impact on overall gauge performance. Gauge measurement error remained below 5% in all instances. This finding suggests the HTS gauge can be utilized over a variety of coolant conditions, providing flexibility to end-users. It is noted, however, that it is recommended to follow manufacturer recommended coolant conditions during characterization and gauge use to prevent damage or invalidation of characterization.

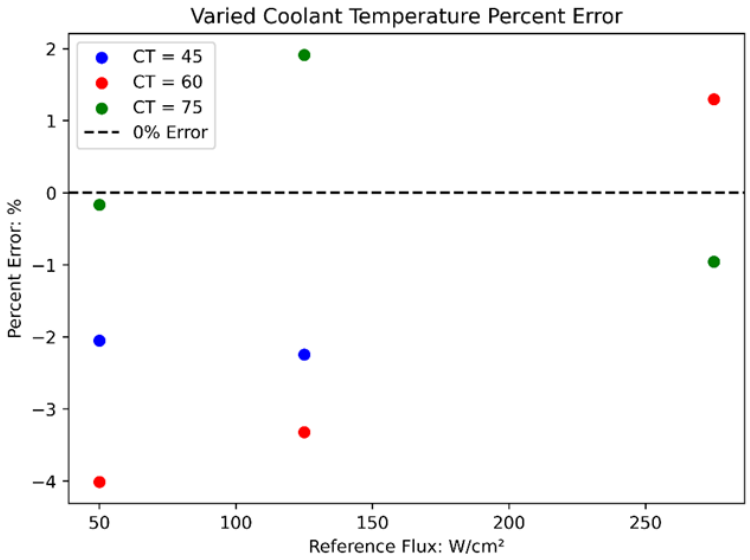

Figure 27. *Constant flow rate 0.3 gpm, varied coolant temperature investigation. Percent error vs flux level.*

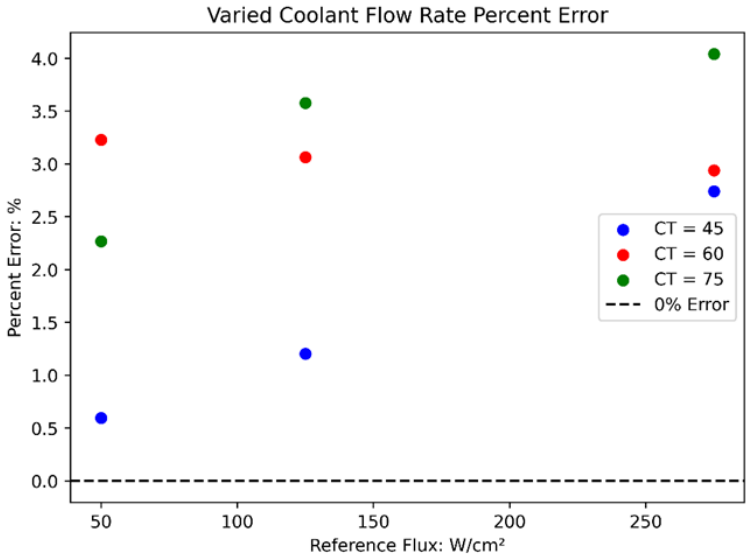

Figure 28. *Constant flow rate 0.1 gpm, varied coolant temperature investigation. Percent error vs flux level.*

4. Prolonged Exposure

The fourth test campaign was designed to evaluate gauge performance under prolonged exposure to high flux levels. The objective was to determine whether extended durations of high flux exposure would adversely affect the internal temperature of the gauges or compromise the integrity of their general assembly. Following a several sequential 10-miute long-duration exposure runs, the results indicated that there were no significant issues related to internal gauge temperature, gauge sensitivity, or coating surface temperature. Figure 29 illustrates the internal gauge temperature throughout the duration of the test, demonstrating a consistent reading. Any observed variations in temperature with time are likely caused by variations in solar conditions over the extended exposure duration. These findings suggest that the gauges are capable of withstanding extended high flux exposure without detrimental effects, thereby affirming their reliability for long-term applications.

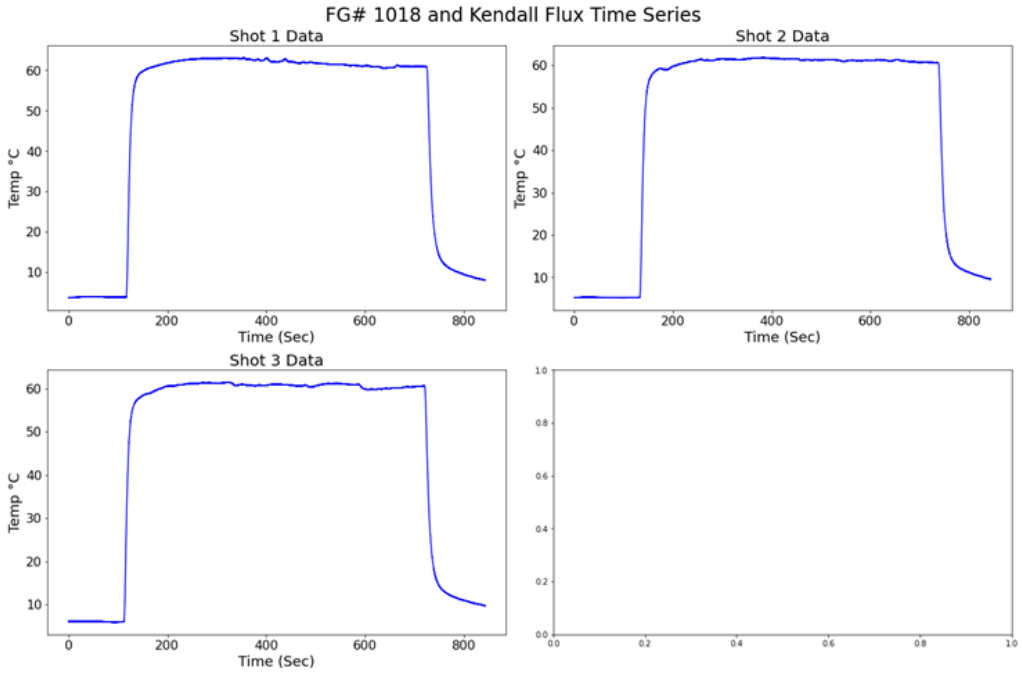

Figure 29. *Long exposure gauge time series showing gauge body temperature vs time.*

5. Coating Thickness

The fifth and final test campaign focused on investigating the re-application of coatings, specifically examining the thickness and its impact on coating temperature and degradation. In certain cases, HTS Gardon gauge products are recoated prior to recharacterization if the gauges have experienced an over-flux incident. While specific coating thickness values are not disclosed here due to confidentiality, general trends are reported.

At the NSTTF, gauges were recoated with both "thicker" and "thinner" paint layers, while the thinner application was intended to capture the thickness applied in the HTS manufacturing process. Subsequently, gauges were subjected to several sequential series of increasing flux levels: 50, 125, and 275 W/cm². The first series aimed to quantify the coating temperature and sensitivity (voltage/flux) during the initial exposure of a fresh coating to high flux. The subsequent series sought to identify any differences from the first series at 50 and 125 W/cm^2, highlighting changes in coating properties.

It was observed that thinner coatings are preferred for mitigating degradation under high flux exposure. Notably, gauges with thicker coatings exhibited significantly higher surface temperatures compared to those with thinner applications. A comparison of Figure 30 and Figure 31 illustrates the temperature and degradation differences associated with varying coating thicknesses. Degradation or changes in properties were indicated by a spike in the IR camera measured coating temperature upon reaching a specific flux level, followed by a noticeable decrease. This suggests that the heat at the surface of the thicker coating was not being absorbed into the body of the gauge as efficiently as the heat on the surface of a thinner coating, resulting in a high temperature oxidative alteration of the coating optical properties.

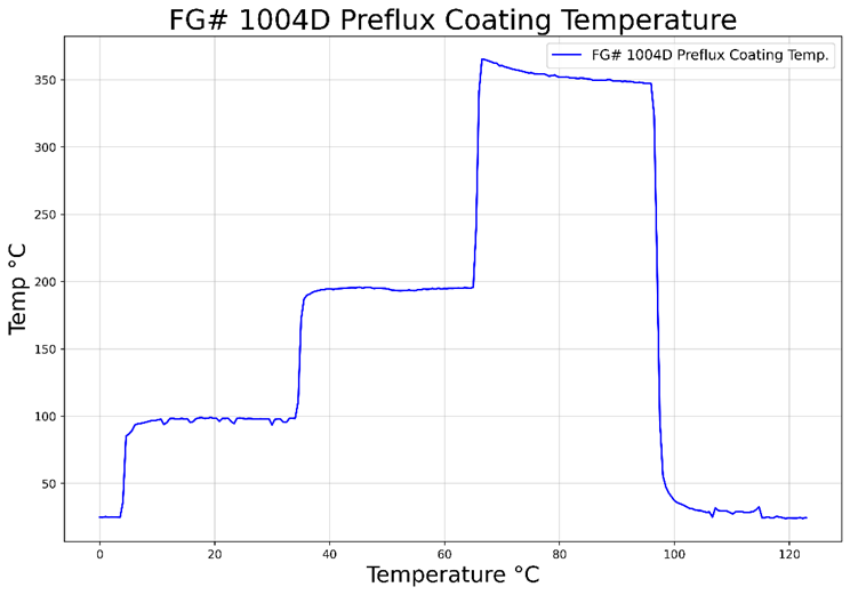

Figure 30. *Coating temperature time series of a gauge with a thinner coating thickness.*

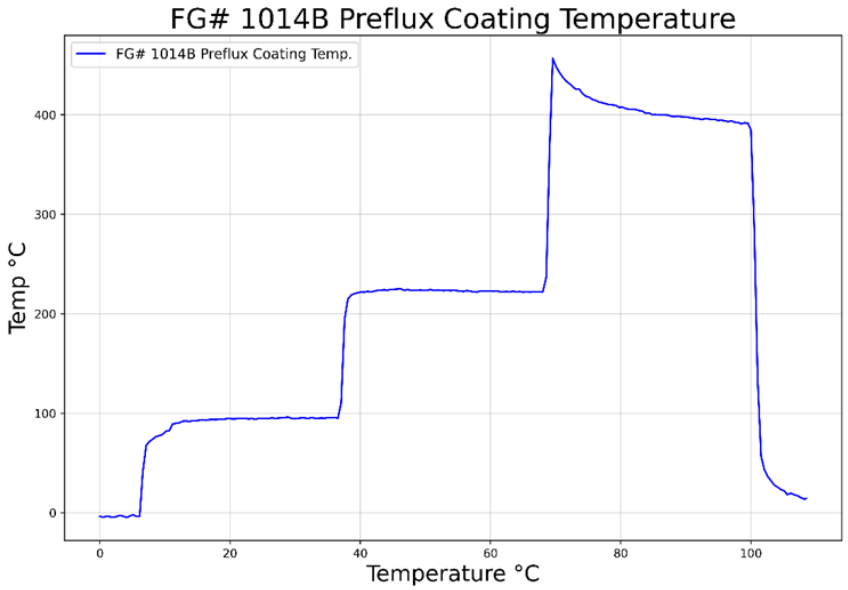

Figure 31. *Coating temperature time series of a gauge with a thinner coating thickness.*

Gauge sensitivities were calculated at the 50 and 125 W/cm^2 flux levels for both the first series of flux exposures and the subsequent series, with results shown in Figure 32 and Figure 33. The gauge with the thinner coating exhibited random variations in sensitivity at each flux level between the initial exposure and the following exposures. In contrast, the gauge with the thicker coating consistently demonstrated lower sensitivity after high flux exposure across all flux levels. As previously mentioned, the gauges exhibited generally lower sensitivities at 50 W/cm² compared to 100 W/cm², irrespective of whether the exposure was initial or subsequent. This observation underscores the potential non-linearity in the gauge's performance at lower flux levels, further reinforcing the conclusion that the optimal operating range for this product lies between 100 and 250 W/cm².

Together, these findings suggest that all gauges should be coated with thinner than thicker coatings. When characterizing or calibration a gauge, it is recommended that gauges with fresh coating should be subjected to their full range of measurable fluxes prior to characterization. This exposure allows for any changes in coating emissivity and thermal properties to occur before characterization, as such changes can significantly impact gauge response. The authors note that too thin of a coating may result in imperfect sealing of the foil, resulting in undesired spectral influences induced by measurement directly on the constantan foil, as well as reduced sensitivity and increased noise.

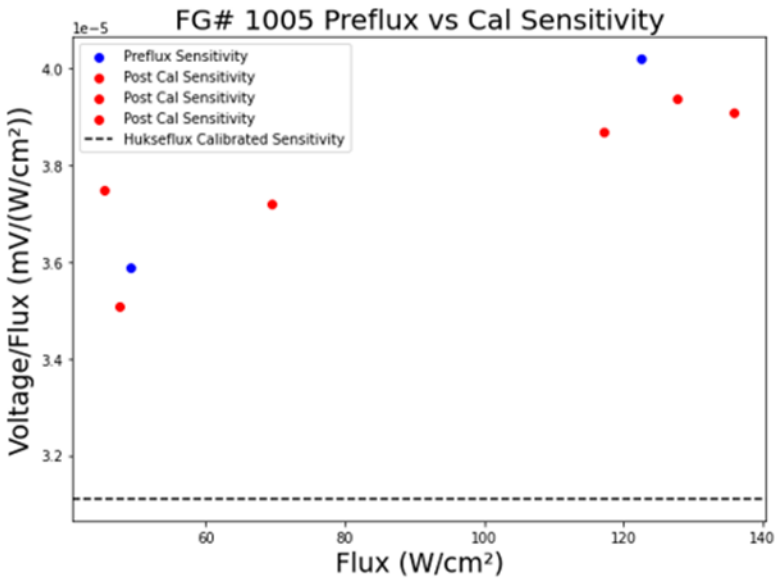

Figure 32. *Before and after pre-flux exposure sensitivity of gauge* with thinner coating.

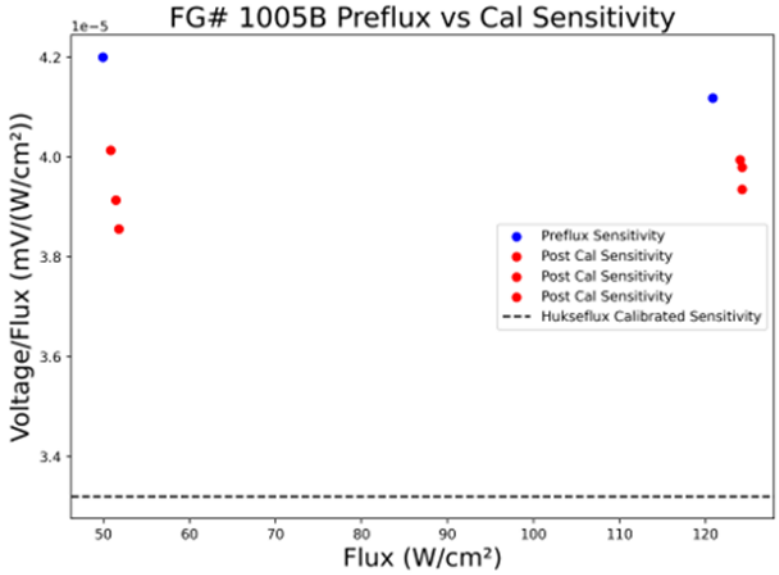

Figure 33. *Before and after pre-flux exposure sensitivity of gauge* with thicker coating.

CONCLUSION

In conclusion, the collaboration between Sandia National Laboratories and Hukseflux Thermal Sensors has successfully advanced the design and characterization of high-intensity heat flux gauges capable of measuring up to 2500 kW/m². This initiative originated from an industry trade study that highlighted the need for improved gauge designs and calibration methodologies specifically tailored for high-intensity and broadband flux applications. Through the development, testing, and evaluation of three prototype gauge designs and four distinct coating

types, we refined our focus to a final product design that incorporates enhanced features for increased robustness under high flux exposure.

The project culminated in a comprehensive testing and characterization campaign, during which the final specifications for the 2500 kW/m² product were established. In addition to gauge development, we upgraded the NSTTF FGCF hardware and characterization methodology to facilitate traceable reference sensor measurements. Enhancements were also made to infrared imaging, coolant flow rate monitoring, and cloud monitoring capabilities, significantly improving the facility's overall effectiveness and operational efficiency. Furthermore, we successfully updated and submitted a publication proposing a high-intensity heat flux calibration method utilizing concentrated solar light, thereby contributing valuable insights and methodologies to the field of heat flux measurement.

The achievements of this project not only address the immediate demands for advanced heat flux measurement but also lay the groundwork for future innovations in the field, particularly as SNL continues to pursue traceability and accreditation within the FGCF. The findings and methodologies developed through this initiative will serve as a vital resource for ongoing research and development in high-intensity heat flux applications.

LIST OF PUBLICATIONS FROM THIS PROJECT

a) *"A proposed high-intensity radiometer calibration method using concentrated solar radiation,"* https://doi.org/10.1016/j.solener.2025.113798, *October 2025.*
b) *"Development of Readily Available and Robust High Heat Flux Gardon Gauges,"* https://doi.org/10.52825/solarpaces.v2i.892, *August 2024*
c) *"Flux Sensor Development and Calibration for Concentrating Solar Power Research and Commercial Heat,"* https://doi.org/10.52825/solarpaces.v1i.637, *April 2024*
d) *"Stability Assessment of High Temperature Coatings for Flux Measurement Applications,"* https://doi.org/10.1115/ES2023-107402, *September 2023*
e) *"Solar Flux Sensor Development and Calibration for Commercial Concentrating Solar Power Research and Application,"* https://www.osti.gov/servlets/purl/2003052, *June 2022.*

REFERENCES

[1] *L. McLaughlin et al., "Flux Sensor Measurement and Calibration Require-ments for High-Intensity Heat Flux Applications," in SolarPACES 2022, Albuquerque, NM, 2022.*
[2] *L. McLaughlin, H. Laubscher, J. Nguyen, L. Banh, and J. Konings, "Development of Readily Available & Robust High Heat Flux Gardon Gauges," SolarPACES Conference Proceedings, 2023.*
[3] *G. P. Mulholland, I. J. Hall, R. M. Edgar, and C. R. Maxwell, "Calibration Procedure for Flux-Gages Used in Solar Environments."*
[4] *E. Guillot, I. Alxneit, J. Ballestrin, J. L. Sans, and C. Willsh, "Comparison of 3 heat flux gauges and a water calorimeter for concentrated solar irradiance measurement," in*

Energy Procedia, 2014, vol. 49: Elsevier Ltd, pp. 2090-2099, doi: 10.1016/j.egypro.2014.03.221.

[5] L. P. McLaughlin, H. Laubscher, and J. Konings, "Stability Assessment of High Temperature Coatings for Flux Measurement Applications," 2023. [Online]. Available: https://doi.org/10.1115/ES2023-107402.

[6] A. Ambrosini, A. Boubault, C. K. Ho, L. Banh, and J. R. Lewis, "Influence of application parameters on stability of Pyromark® 2500 receiver coatings," vol. 2126, ed: American Institute of Physics Inc., 2019.